Mechanical modeling of metallic strands subjected to tension, torsion and bending.

Francesco Foti[1], Luca Martinelli

Politecnico di Milano
Department of Civil and Environmental Engineering
P.zza L. da Vinci 32, 20133 Milano

Abstract

Aim of the present work is to build a link between a structural theory for large-scale analyses of three-dimensional cable structures undergoing, in general, large displacements and rotations, and a refined mechanical description of metallic strands, fully accounting for their composite nature and hysteretic bending behavior.

A new formulation for metallic strands is presented. The strand overall mechanical behavior is modeled according to the Euler-Bernoulli beam theory. A constitutive law relating the cross sectional generalized stresses and strains of the adopted structural model is obtained by summing over the individual contributions of wires.

Each wire in the strand is individually modeled as a curved thin rod. Kinematic equations are proposed to relate the wire generalized strain variables to those of the strand cross section. The equilibrium of the individual wires is analyzed under the hypothesis of radial contact between adjacent layers taking, most notably, also into account the effects due to the residual radial contact forces induced by the strand manufacturing process. Deformations of contact surfaces are neglected and friction is accounted for, through the Amontons-Coulomb law, in the study of the stick-slip conditions.

The proposed sectional model accounts for some distinctive characteristic aspects of wire ropes, such as the coupling between axial force and torque and the non-linear,

Email addresses: francesco.foti@polimi.it (Francesco Foti), luca.martinelli@polimi.it (Luca Martinelli)
[1]Corresponding author

and non-holonomic, relation between bending moment and curvature, which is a consequence of sliding of wires.

The performance of the proposed formulation is assessed with reference to well-documented physical tests and established analytical formulations. Moreover, the role of the residual contact forces due to the stranding process, on the bending behaviour of a typical multi-layer strand is assessed.

Keywords: Strands, Cyclic bending, Corotational finite element, Contact forces, Wire sliding, Friction

---

1. Introduction

Metallic strands are widely employed structural members. They are used in many different engineering applications, due to their good electric conductivity, e.g. overhead transmission lines, and their ability in carrying high tensile forces with relatively small deadloads, e.g.: tensile structures, guyed masts and towers, stays and suspension cables. Furthermore, they can be regarded as the basic components of metallic wire ropes, which are largely used in lifting devices, offshore anchoring systems and suspended bridges. Strands are made of helical wires, which are twisted around an initially straight core and grouped in concentric layers. Wire ropes, in turn, are obtained by helically twisting and grouping metallic strands. The wire stranding, hence, can be regarded as the basis of a recursive manufacturing procedure to obtain complex multi-component elements with a hierarchical helical internal structure. More details on the metallic strand construction can be found e.g. in: (Feyrer, 2007; Rawlins, 2005), while an insight into the geometric modeling of helical assemblies has been provided, e.g., by Lee (1991), Wang et al. (2015).

Large scale structural analyses are often performed by modeling strands as perfectly flexible elements, reacting only to axial forces. The static and dynamic response of such elements have been thoroughly investigated both with analytical (see e.g.: Irvine, 1981; Rega, 2004), as well as with numerical techniques (e.g.: Migliore and Webster 1979, 1982; Martinelli and Perotti, 2001). Sometimes, however, to correctly represent some important features of the strand mechanical response it can be

necessary to overcome the perfectly flexible structural model, by taking into account bending and torsional stiffness contributions. These beam-like stiffness terms, in fact, allow to model the characteristic coupling between axial and torsional behaviour (McConnell and Chang, 1986), which in real strands is a direct consequence of the internal structure. Besides, these can play an important role in "critical" regions, such as in the neighborhood of constraints, and in modeling slack cable structures (Lacarbonara and Pacitti, 2008; Zhu and Meguid 2006). In "critical" regions, in fact, the stress-strain state of the strands can differ significantly from the pure tension one. Finally, an accurate modeling of the strand bending moment-curvature relations can be important to simulate flexural vibrations, which are characterized by an hysteretic damping mechanism as it can be inferred from both static (Papailiou, 1997; Chen et al., 2015) and dynamic tests (Zhu and Meguid, 2007).

The hysteretic bending behavior of strands is inherently related to the interactions among adjacent wires which can occur at internal contact surfaces. Here friction forces tend to contrast relative interwire displacements, allowing for the transmission of tangential stresses between contacting wires, during the bending of the strand. When the forces activating the sliding are greater than friction, a wire can undergo a relative displacement with respect to the neighbors ones. This friction-based mechanism for the transmission of shearing stresses, while providing the required flexibility for many structural applications, makes the strand bending behavior non-linear. The power dissipated because of internal sliding contributes to self-damping of the elements. This, in turn, plays a key role in assessing the vibration level of lightly damped structures, such as suspended cables (e.g.: Goudreau et al., 1998; Rawlins, 2009), as well as the performance of damping and base isolation devices (e.g.: Gerges, 2008; Sauter and Hagedorn, 2002). Moreover, interwire sliding is related to fretting fatigue and wear phenomena that significantly affect the service life of strands and wire ropes, as it has been clearly pointed out by the results of several experimental tests (Giglio and Manes, 2003; Winkler et al., 2015; Urchegui et al., 2008).

Classic two- and three-dimensional beam theories have been recently adopted to study the flexural vibrations of short metallic strands, by Spak et al. (2014) and Oliveto and Sivaselvan (2014) respectively. Both these approaches are quite suitable

for large-scale structural analyses, but, since they rely on the assumption of homogeneous isotropic material, do not allow to capture the previously mentioned complex interwire interactions as well as their effects on the hysteretic bending behavior of metallic cables. These issues, on the other hand, have been studied in the literature which stems mainly from the mechanical engineering field, see e.g. the review papers by Cardou and Jolicoeur (1997), Cardou (2006) and the more recent one by Spak et al. (2013), especially focused on internal damping mechanisms. Most of the mechanical models proposed in the mechanical engineering field, however, are conceived so as to perform local stress-strain analyses, or for the solution of particular problems (e.g. strands passing over a pulley).

The Finite Element method has also been used to study metallic strands and wire ropes (e.g.: Jiang et al., 1999; Judge, 2012). Full three-dimensional FE formulations, however, while providing invaluable tools to investigate complex local mechanical phenomena, cannot be successfully applied to large-scale structural analyses because of the huge computational costs related to the size of the models.

The aim of the present work is to build a link between a structural theory for large-scale analyses of three-dimensional cable structures undergoing, in general, large displacements and rotations, and a refined description of metallic strands, fully accounting for their nature of composite structural materials and the hysteretic bending behavior.

A first attempt in this direction has already been given by Papailiou, who in a seminal paper (Papailiou, 1997) studied a strand subjected to a combination of axial force and uniform bending to derive a multi-linear cross sectional moment-curvature relation. Analytical expressions allow to evaluate, for a given value of the strand axial force, the critical values of the curvatures and moments at the kinks of the first loading branch of the curve. Hence, if the axial force of the element is assumed constant during the analysis, the strand cross sectional response can be evaluated similarly to the case of a beam with an elasto-plastic multilinear moment-curvature law. Indeed, Papailiou, implemented its model into a simple research FE code for the non-linear static analysis of planar beams assemblies and compared the numerical results with quasi-static experimental test, showing a good qualitative agreement between predictions of the model and experiments. Later in time, Dastous (2005) adopted the Papailiou's model

to study the static and dynamic response of short span substation conductors. Inagaki et al. (2007), instead, extended Papiliou's model to study the stresses and the occurrence of interwire sliding in complex electrical cables used in robot applications, subjected to a combination of axial-torsional loads and planar bending. To this aim, these authors generalized the Papailiou's analysis to the case of hierarchical helical structures. As a major simplification, however, they neglected torsional and bending stresses of the wires in evaluating the global response of the assembly.

Papailiou's model has been also slightly modified by Hong et al. (2005), which reconsidered the calculation of the contact forces, and, more recently by Paradis and Légeron (2011), which accounted for the tangential compliance of internal contact surfaces. The latter model has been adopted, then, by Langlois et al. (2014) to study the planar vibrations of an overhead conductor. It's worth noting that all the aforementioned models are confined to the case of planar vibrations of tensioned strands, but predict a linearly elastic response for slack cables which is in contrast with experimental findings, see e.g.: (Zhu and Meguid, 2007; Chen et al., 2015).

In the present paper a new three-dimensional (3-D) formulation for strands made of metallic wires is presented. The strand overall mechanical behavior is modeled according to the Euler-Bernoulli beam theory. A constitutive law relating the cross sectional generalized stresses and strains of the adopted structural model is obtained by summing over the individual wires contributions.

Each wire in the strand is individually modeled according to the Kirchhoff-Clebsch-Love (KCL) theory of curved thin rods (Love, 1944) starting from a mathematical description of the internal structure. Kinematic equations are proposed to relate the wire generalized strain variables to those of the strand cross section under the assumption that the cross sections of the wires rotate rigidly with the cross section of the strand. The equilibrium of the individual wires is then analyzed under the hypothesis of radial contact between adjacent layers, most notably taking also into account the clenching effect due to the residual radial contact forces induced by the manufacturing of the strand.

Deformations of contact surfaces are neglected and friction is accounted for through the classic Amontons-Coulomb model. Accordingly, the stick-slip conditions are stud-

ied and an incremental procedure, based on an operator split into a frictional stick part and a frictional slip part and on a classical Return Map Algorithm, is adopted to calculate the response of each wire.

The proposed sectional model accounts for some characteristic aspects of wire ropes, such as the coupling between axial force and torque and the non-linear, and non-holonomic, relation between bending moment and curvature, which is a consequence of sliding of the wires.

The sectional model has been implemented in a corotational 3-D small-strain beam finite element, able to account for the geometric non-linearities which have not to be neglected in the modeling of cable-like structures.

The performance of the proposed formulation is assessed with reference to well-documented physical tests and established analytical formulations, first for a single-layer steel strand under combined axial-torsional loading, subsequently, with respect to experimental bending tests of a "Galfan coated" steel strand.

Moreover, the role of the residual contact forces associated to the clenching effect due to the stranding process, on the bending behaviour of a typical four-layer stranded electrical conductor (ACSR Curlew 7/54) is assessed.

2. Kinematics of the strand

Metallic strands are made of helical wires, twisted around an initially straight core and arranged in concentric layers, symmetric with respect to the element centerline. The core is usually another wire (*core wire*), which ensures the stability of the assembly by providing a radial support to the external wires.

A mathematical description of the strand kinematics can be conveniently developed within a *Strand-attached Reference System* (SRS), i.e. a right-handed Cartesian frame whose axes $\{x_i\}$ $(i = 1,2,3)$ are defined such that x_1 coincides with the strand centerline (see Figure 1). In the following, the unit vectors of the SRS will be denoted as $\{\mathbf{e}_i\}$.

Assuming the straight strand configuration ideally free from constraints as the reference configuration, strand kinematics can be described according to the classic Euler-Bernoulli beam theory. Under the further assumption of small displacements

and strains, at a generic time t the strand cross sections are characterized by the axial displacement $u_{s1}(x_1,t)$ and the rotation vector $\varphi_s(x_1,t)$, whose components, $\varphi_{si}(x_1,t)$, in the basis $\{\mathbf{e}_i\}$, represent the cross sectional rotations about the SRS axes:

$$\varphi_s(x_1,t) = \sum_{i=1}^{3} \varphi_{si}(x_1,t)\,\mathbf{e}_i \tag{1}$$

Within this context, the axial strain, $\varepsilon_s(x_1,t)$, and the curvature vector, $\chi_s(x_1,t)$, can be defined, respectively, as:

$$\varepsilon_s(x_1,t) = \frac{\partial u_{s1}}{\partial x_1};\;\; \chi_s(x_1,t) = \sum_{i=1}^{3} \chi_{si}(x_1,t)\,\mathbf{e}_i = \frac{\partial \varphi_s}{\partial x_1} \tag{2a, b}$$

3. Geometry of the wire

A generic wire in the strand can be described as a curved thin round rod, by specifying, for each cross section, the position of the centroid and the orientation with respect to the SRS (see Figure 1). It's worth noting, however, that the analytical results presented herein are general and apply also to a different wire cross section (e.g. triangular wires, trapezoidal wires).

The locus of centroids (centerline) can be represented as a circular helix in the SRS, with radius R and pitch P. A positive sign is conventionally assumed, in this work, for the pitch of helices that are twisted around the axis x_1 according to the right-hand rule. To identify the points of the helix, a position vector, $\mathbf{x}_w$, is introduced as a function of the *swept angle*, θ, i.e. the angle which the projection of the position vector on the plane $x_1 = 0$ defines with the axis x_2. By denoting as $\{\mathbf{e}_i\}$ the unit vectors of the SRS and adopting the subscript "0" to identify the value of the swept angle at $x_1 = 0$, the following holds:

$$\mathbf{x}_w(\theta) = \frac{P}{2\pi}(\theta - \theta_0)\,\mathbf{e}_1 + R\cos(\theta)\,\mathbf{e}_2 + R\sin(\theta)\,\mathbf{e}_3 \tag{3}$$

The orientation of the wire cross section, then, can be described by introducing on the wire centerline the local Serret-Frenet unit vectors $\{\mathbf{f}_i(\theta)\}$ $(i = 1,2,3)$, such that: $\mathbf{f}_1(\theta)$ is the tangent vector, while $\mathbf{f}_2(\theta)$ and $\mathbf{f}_3(\theta)$ are, respectively, the normal

and binormal unit vectors of the wire centerline. The Serret-Frenet unit vectors can be easily evaluated starting from equation (3), see e.g. (Kreyzsig, 1991), and related to the unit vectors of the SRS by means of a rotation tensor, $\mathbf{\Lambda}_w(\theta)$, such as:

$$\mathbf{f}_i(\theta) = \mathbf{\Lambda}_w(\theta)\,\mathbf{e}_i,\ i = 1,2,3 \tag{4}$$

By denoting as α the the lay angle of the wire, i.e. the constant angle which the tangent vector $\mathbf{f}_1$ defines with the strand axis x_1, the components of $\mathbf{\Lambda}_w(\theta)$ in the SRS (here denoted as $[\mathbf{\Lambda}_w(\theta)]_{\mathbf{e}}$) can be expressed as it follows:

$$[\mathbf{\Lambda}_w(\theta)]_{\mathbf{e}} = \begin{bmatrix} \cos(\alpha) & 0 & \sin(\alpha) \\ -\sin(\alpha)\sin(\theta) & -\cos(\theta) & \cos(\alpha)\sin(\theta) \\ \sin(\alpha)\cos(\theta) & -\sin(\theta) & -\cos(\alpha)\cos(\theta) \end{bmatrix} \tag{5}$$

It's worth noting that the lay angle α can be related to the helix radius and pitch, R and P, through simple geometric arguments, such that: $\alpha = \tan^{-1}\left(\frac{2\pi R}{P}\right)$. Hence, equations (3)-(5) completely define the geometry of a generic wire as a function of two construction parameters (i.e. R and P) and the angular coordinate θ. Alternative, but equivalent, expressions can be also derived in terms of the cartesian coordinate x_1 (Eq. (6a)) defined on the wire centerline, or an arc-length coordinate S (Eq. (6b)), by considering an infinitesimal segment of the helix:

$$\tan(\alpha)\,dx_1 = Rd\theta;\ \sin(\alpha)\,dS = Rd\theta \tag{6a, b}$$

By integrating the above equations, together with suitable boundary conditions, the swept angle can be expressed as a function of x_1 or S.

The variation of the local vectors $\{\mathbf{f}_i(\theta(S))\}$ along the wire centerline is given by the well known Serret-Frenet equations (see again Kreyszig, 1991), here expressed by highlighting the dependency upon the arc-length coordinate S as:

$$\frac{d\mathbf{f}_1(S)}{dS} = \kappa\mathbf{f}_2(S);\ \frac{d\mathbf{f}_2(S)}{dS} = \tau\mathbf{f}_3(S) - \kappa\mathbf{f}_1(S);\ \frac{d\mathbf{f}_3(S)}{dS} = -\tau\mathbf{f}_2(S) \tag{7a, b, c}$$

The symbols κ and τ denote, respectively, the curvature and torsion of the wire centerline, which can be evaluated as it follows:

$$\kappa = \frac{\sin^2(\alpha)}{R}; \quad \tau = \frac{\sin(\alpha)\cos(\alpha)}{R} \tag{8a, b}$$

The Serret-Frenet formulae can be used also to express the derivative of the rotation tensor $\mathbf{\Lambda}_w(\theta(S))$ with respect to S. Indeed, by recalling (4), the following equation can be easily obtained from (7a, b, c):

$$\frac{d\mathbf{\Lambda}_w(S)}{dS} = \mathbf{\Lambda}_w(S)\,\mathbf{\Omega}_{w,ref} \tag{9}$$

having denoted as $\mathbf{\Omega}_{w,ref}$ a skew-symmetric tensor whose components (here denoted as $\left[\mathbf{\Omega}_{w,ref}\right]_{\mathbf{f}}$) in the local basis $\{\mathbf{f}_i\}$ can be expressed as:

$$\left[\mathbf{\Omega}_{w,ref}\right]_{\mathbf{f}} = \begin{bmatrix} 0 & -\kappa & 0 \\ \kappa & 0 & -\tau \\ 0 & \tau & 0 \end{bmatrix} \tag{10}$$

4. The wire mechanical model

Strands can be modeled as composite structural elements, starting from a description of the mechanical behavior of their basic components. Within this context, wires can be considered as curved thin rods.

In this work, wires are described according to the classic Kirchhoff-Clebsch-Love (KCL) theory for elastic curved thin rods (Love, 1944) under the further assumption of small displacements and rotations of the cross sections. Consequently, cross sections remain plane and normal to the deformed centerline of the rod and a linear strain measure is assumed at the continuum level. Shear deformability is considered negligible due to the inherent slenderness and flexibility of typical metallic wires. Moreover, in order to define a constitutive model suitable for large-scale structural analyses, variations of the strand internal geometry with respect to the reference (undeformed) configuration are disregarded.

The mechanical response of wires can be conveniently studied within a moving reference frame centered on the centroid of the cross section and with axes directed as the Serret-Frenet unit vectors, $\{\mathbf{f}_i(S)\}$ $(i=1,2,3)$, function of the arc-length coordinate S, defined in Section 3. It's worth also noting that vectors $\{\mathbf{f}_i\}$ identify a set of principal axes for round wire cross sections. Within this framework, the generalized stresses of the curved thin rod model are defined as the axial force, F_{w1}, and the moments acting with respect to the directions of the vectors $\{\mathbf{f}_i\}$, i.e. the torsional moment M_{w1} and the bending moments M_{w2} and M_{w3}. The generalized, work-conjugated, cross sectional strains are the wire axial strain ε_w (i.e. the elongation of the wire centerline) and the mechanical curvatures χ_{wi} $(i=1,2,3)$, which can be conveniently collected into the vector $\boldsymbol{\chi}_w(S)=\sum_{i=1}^{3}\chi_{wi}(S)\mathbf{f}_i(S)$, and expressed as a function of the wire cross sectional rotation, of its derivative with respect to the arc-length coordinate S, and of the initial curvature (κ) and torsion (τ) of the undeformed centerline (see Section 3, equations (8a, b)). To this aim, the kinematic equations proposed by Huang (1973) are adopted in this work. Here they will be re-written, with a more concise matrix notation, as it follows:

$$\boldsymbol{\chi}_w=\frac{d\boldsymbol{\varphi}_w}{dS}+\boldsymbol{\Omega}_{w,ref}\boldsymbol{\varphi}_w;\;\; \boldsymbol{\varphi}_w(S)=\sum_{i=1}^{3}\varphi_{wi}(S)\mathbf{f}_i(S) \qquad (11a, b)$$

where $\boldsymbol{\Omega}_{w,ref}$ is the skew-symmetric tensor defined in equation (10) and $\boldsymbol{\varphi}_w(S)$ is a vector whose components, $\varphi_{wi}(S)$, in the basis $\{\mathbf{f}_i\}$, represent the cross sectional rotations about the moving reference system of the wire.

The constitutive equations can be defined by following Love's formulation (Love, 1944) for linearly elastic curved thin rods, under the further assumption of circular symmetry of the cross section (e.g. round cross section):

$$F_{w1}=EA_w\varepsilon_w;\;\; M_{w1}=\frac{EI_w}{1+\nu}\chi_{w1};\;\; M_{w2}=EI_w\chi_{w2};\;\; M_{w3}=EI_w\chi_{w3} \qquad (12a, b, c, d)$$

Here, E and ν are the Young modulus and the Poisson coefficient of the wire material, while A_w and I_w denote, respectively, the area and the second area moment of the wire cross section about its principal inertia axes.

Finally, the indefinite equilibrium equations of the wire under the action of a generic system of external forces ($\mathbf{t}(S)$) and couples ($\mathbf{m}(S)$) per unit length of the wire centerline, can be written as (see e.g. Love, 1944):

$$\frac{d\mathbf{F}_w}{dS} + \boldsymbol{\Omega}_{w,ref}\mathbf{F}_w + \mathbf{t} = \mathbf{0}; \quad \frac{d\mathbf{M}_w}{dS} + \boldsymbol{\Omega}_{w,ref}\mathbf{M}_w + \mathbf{f}_1 \times \mathbf{F}_w + \mathbf{m} = \mathbf{0} \tag{13a, b}$$

where: $\mathbf{F}_w(S) = \sum_{i=1}^{3} F_{wi}(S)\mathbf{f}_i(S)$, $\mathbf{M}_w(S) = \sum_{i=1}^{3} M_{wi}(S)\mathbf{f}_i(S)$, and $\times$ denotes the vectorial (cross) product.

It's worth noticing that since the shear force components F_{w2} and F_{w3}, acting in the wire cross section, are not generalized stresses of the model they can be only evaluated a-posteriori by solving the equilibrium equations (13a, b), should they be required.

5. Evaluation of the wire strains

The deformation of a generic wire can be defined relating the strand strains, ε_s and χ_s in equations (2a, b), to the generalized strain variables of the KCL theory introduced in Section 4.

To this aim, it can be convenient to consider separately the elongation and the curvatures of the wire.

5.1. Wire axial strain

By neglecting changes in the strand internal geometry with respect to the reference configuration, the wire axial strain can be expressed as the sum of three terms, stemming respectively from the axial-torsional deformation of the strand ($\varepsilon_{w,at}$), and from the bending of the strand about axes x_2, and x_3 ($\varepsilon_{w,b2}$ and $\varepsilon_{w,b3}$):

$$\varepsilon_w(S,t) = \varepsilon_{w,at}(S,t) + \varepsilon_{w,b2}(S,t) + \varepsilon_{w,b3}(S,t) \tag{14}$$

Let us consider first the axial-torsional contribution $\varepsilon_{w,at}$. Under the hypothesis of excluding the breaking of wires (axisymmetric element), a combination of axial load and torsional moment applied at the end sections of the strand leads to an axisymmetric mechanical problem. As a consequence, all wires belonging to the same concentric

layer behave identically, and the stress-strain state of a generic wire is constant along its length. This obviously simplifies the evaluation of the response and, in particular, the analysis of the deformative process of the wires, whose centerline is transformed into a circular helix, possibly characterized by different radius and pitch with respect to the reference configuration, but still having the strand centerline as axis of revolution (see e.g. Costello, 1990).

This hypothesis of preservation of the wire helicoidal geometry was adopted by Lanteigne (1985) to study the axial-torsional behavior of the strand, and considering small strains and negligible changes in the internal geometry of the strand he derived the following linear kinematic equation:

$$\varepsilon_{w,at}(S,t) = \cos^2(\alpha)\,\varepsilon_s(x_1(S),t) + R\sin(\alpha)\cos(\alpha)\,\chi_{s1}(x_1(S),t) \tag{15}$$

It's worth noting that the above equation gives a constant solution under the hypothesis of uniform axial strain and torsion of the strand, which is in agreement with the symmetry requirements of the basic axial-torsional loading case previously discussed.

Let's consider now the contributions $\varepsilon_{w,b2}$ and $\varepsilon_{w,b3}$ due to bending of the strand. Two limit kinematic assumptions have been proposed in literature (see e.g. Cardou and Jolicoeur, 1997; Cardou, 2006), which will be referred in the following respectively as the the *slip-state* and the *stick-state* assumptions. In the first case, the strand is modeled as a bundle of individually bent components. The wire length remains unchanged and the displacements in the direction of the strand axis, x_1, are proportional to the distance from a wire diameter parallel to the strand neutral axis of bending. As a consequence, the bending contribution to the axial strain of the wires is strictly equal to zero.

Under the stick-state hypothesis, instead, the wires are assumed as a part of an "ideal" strand cross section, planar and normal to the deformed strand centerline, according to the Euler-Bernoulli kinematic model. The wire displacements along the SRS axis x_1, hence, are proportional to the wire distance from the neutral axis of bending of the strand. Under the stick-state assumption, accounting for the angle α between wire and strand centerline, the bending contributions to the wire axial strain are easily

evaluated as:

$$\begin{aligned} \varepsilon_{w,b2}^{stick}(S,t) &= R\cos^2(\alpha)\sin(\theta(S))\,\chi_{s2}(S,t) \\ \varepsilon_{w,b3}^{stick}(S,t) &= R\cos^2(\alpha)\cos(\theta(S))\,\chi_{s3}(S,t) \end{aligned} \qquad (16a, b)$$

where the dependence of the trigonometric functions argument on the arc-length coordinate S has been emphasized.

Equations (16a, b), which are first proposed herein, can be regarded as a generalization to the biaxial bending case of the stick-state kinematic relations already proposed in classic models (see e.g. Lanteigne, 1985; Papailiou, 1997) for the planar bending of strands.

Equations (16a, b) predict, in the stick-state, a variable wire axial strain. This, in turn, is related to a variable wire axial force through the constitutive equations introduced in Section 4 (see Eq. (12(a))). Because of the consequent axial force gradient, wires tend to slip relatively to one another. Slipping is contrasted by friction forces that develop at the contact surfaces as a function of the internal geometry of the strand, of the material properties of its components and of the *intra-* and *inter-layer* contact forces. Hence, during the deformative process, a generic wire can fulfill the stick-state assumption only as long as the friction forces are large enough to counterbalance the effect of the axial force gradient. Otherwise, the wire undergoes a relative displacement with respect to the neighbors, and has to be considered as individually bent according to the slip-state kinematic model.

The bending of the strand, hence, is an inherently non-linear problem, and the kinematic equations for $\varepsilon_{w,b2}$ and $\varepsilon_{w,b3}$ can be more properly stated in a rate (or incremental) form. To this aim, having denoted with a dot the derivative with respect to time, the following alternative relations are introduced, which account for the actual state of the wire:

$$\dot{\varepsilon}_{w,bi}(S,t) = \left\{\text{sticking}:\ \dot{\varepsilon}_{w,bi}^{stick}(S,t);\ \text{slipping}:\ 0\right\},\ \text{with}:\ i=2,3 \qquad (17)$$

At a generic time, the total axial strain due to bending contributions is then a function of the past history of the strand, and can be defined through the following integral

equation:

$$\varepsilon_{w,bi}(S,t) = \int_0^t \dot{\varepsilon}_{w,bi}(S,t)\,dt, \;\; \text{with}: \; i = 2,3 \tag{18}$$

5.2. Wire curvatures

A new procedure to compute the wire curvatures is presented in this Section, based on the assumption that the wire cross section rotates rigidly with the cross section of the strand. The following equation can be introduced to relate the rotation vector of the strand, φ_s, to that of a wire, φ_w (see also equations (1) and (11b) for the definitions):

$$\varphi_w(S,t) = \mathbf{\Lambda}_w^T(S)\,\varphi_s(x_1(S),t) \tag{19}$$

where $\mathbf{\Lambda}_w$ is the rotation tensor which gives the orientation of the Serret-Frenet unit vectors of the wire with respect to the SRS.

In order to evaluate the derivative of (19) with respect to S, it's worth noting that from equations (6a, b), the following differential relation can be easily obtained: $dx_1 = dS\cos(\alpha)$. Hence, by recalling the definition of strand curvatures given in (2b), we get:

$$\frac{\partial \varphi_w}{\partial S} = \cos(\alpha)\,\mathbf{\Lambda}_w^T(S)\,\chi_s(x_1(S),t) + \frac{d\mathbf{\Lambda}_w^T}{dS}\varphi_s(x_1(S),t) \tag{20}$$

By solving equation (19) for φ_s and substituting in (20), and recalling (9), the following equation is then obtained:

$$\frac{\partial \varphi_w}{\partial S} = \cos(\alpha)\,\mathbf{\Lambda}_w^T(S)\,\chi_s(x_1(S),t) - \mathbf{\Omega}_{w,ref}(S)\,\varphi_w(S,t) \tag{21}$$

The latter result can be used together with the definition given in equation (11a) to evaluate the wire curvatures as:

$$\chi_w(S,t) = \cos(\alpha)\,\mathbf{\Lambda}_w^T(S)\,\chi_s(x_1(S),t) \tag{22}$$

6. Strand cross sectional response

According to the kinematic model defined in the previous Section, the mechanical response of the strand cross section can be described in terms of the resultant axial force, $N_s(x_1,t)$, the torsional moment, $M_{s1}(x_1,t)$ and the bending moments $M_{si}(x_1,t)$, $(i=2,3)$. The virtual work per unit of length of the strand, δW_s, is then expressed as:

$$\delta W_s = N_s \delta \varepsilon_s + \sum_{i=1}^{3} M_{si} \delta \chi_{si} = \sigma_s^T \delta \varepsilon_s \tag{23}$$

where the column vectors σ_s and ε_s have been introduced to collect the work-conjugated stress and strain variables of the strand, i.e: $[\sigma_s] = [N_s, M_{s1}, M_{s2}, M_{s3}]^T$ and $[\varepsilon_s] = [\varepsilon_s, \chi_{s1}, \chi_{s2}, \chi_{s3}]^T$.

6.1. Stress resultants

The strand resultant axial force and moments can be evaluated through simple equilibrium considerations, by summing all wire contributions. To this end the axial force of a wire, F_{w1}, is projected on the strand reference system (SRS), obtaining the vector:

$$\mathbf{F}_{wp} = F_{w1}(\cos(\alpha)\,\mathbf{e}_1 - \sin(\alpha)\sin(\theta)\,\mathbf{e}_2 + \sin(\alpha)\cos(\theta)\,\mathbf{e}_3) \tag{24}$$

Vector $\mathbf{F}_{wp}$ is given by the sum of the out-of-plane term $F_{w1}\cos(\alpha)$ and the in-plane contribution $F_{w1}\sin(\alpha)$, normal to the helix radius R. Having denoted as m the number of layers, as n_j the number of wires belonging to the j^{th} layer, and having reserved the subscript "0" to quantities referred to the core of the strand, the strand axial force can be simply evaluated by summation:

$$N_s = \sum_{j=0}^{m} \sum_{i=1}^{n_j} F_{w1,ij} \cos(\alpha_j) \tag{25}$$

The strand resultant moments can be similarly evaluated by first projecting the wire moments on the SRS and then adding the contribution stemming from the vector $\mathbf{F}_{wp}$:

$$M_{s1} = \sum_{j=0}^{m} \sum_{i=1}^{n_j} c(\alpha_j) M_{w1,ij} + s(\alpha_j) M_{w3,ij} + R_j s(\alpha_j) F_{w1,ij} \tag{26}$$

$$M_{s2} = \sum_{j=0}^{m} \sum_{i=1}^{n_j} -s(\alpha_j)\, s(\theta_i)\, M_{w1,ij} - c(\theta_i)\, M_{w2,ij} + c(\alpha_j)\, s(\theta_i)\, M_{w3,ij} + R_j c(\alpha_j)\, s(\theta_i)\, F_{w1,ij} \tag{27}$$

$$M_{s3} = \sum_{j=0}^{m} \sum_{i=1}^{n_j} s(\alpha_j)\, c(\theta_i)\, M_{w1,ij} - s(\theta_i)\, M_{w2,ij} - c(\alpha_j)\, c(\theta_i)\, M_{w3,ij} - R_j c(\alpha_j)\, c(\theta_i)\, F_{w1,ij} \tag{28}$$

where $s(\cdot)$ and $c(\cdot)$ denote, respectively, the sine and cosine functions.

6.2. Tangent stiffness matrix

Within the state determination procedure of a non-linear displacement-based beam finite element formulation, it is important to evaluate the tangent stiffness matrix, $\mathbf{K}_s$, which relates the variations of the generalized cross sectional stress and strain variables: $\delta\sigma_s = \mathbf{K}_s \delta\varepsilon_s$. By its very definition, the matrix $\mathbf{K}_s$ can be calculated by taking the derivatives of the stress-strain relations (equations (25)-(28)) with respect to the strain variables, i.e., with a concise notation:

$$\mathbf{K}_s = \frac{\partial \sigma_s}{\partial \varepsilon_s} \tag{29}$$

Under the assumption of linearly elastic behavior of the wires (constitutive equations (12)), it can be easily shown that the non-linearities in equations (25)-(28) are only due to the contribution of the wire axial strain components which are due to the strand bending (see equations (17) and (18)). Moreover, it is possible to express the cross sectional tangent stiffness as the sum of a constant contribution, $\mathbf{K}_{s,slip}$, evaluated under the assumption of full-slip bending behavior of wires, and an additional term, $\mathbf{K}_{s,add}$, which can vary during the analysis and accounts for the evolution of the interwire sliding phenomena. I.e.:

$$\mathbf{K}_s = \mathbf{K}_{s,slip} + \mathbf{K}_{s,add} \tag{30}$$

After some straightforward calculation, the constant contribution $\mathbf{K}_{s,slip}$ can be expressed as:

$$\mathbf{K}_{s,slip} = \begin{pmatrix} EA & C_{AT} & & \\ C_{AT} & GJ & \mathbf{0}_{2\times 2} & \\ & & EI_{\min} & 0 \\ \mathbf{0}_{2\times 2} & & 0 & EI_{\min} \end{pmatrix} \tag{31}$$

where EA, GJ and $EI_{\min}$ denote, respectively the axial, torsional and bending direct stiffness terms, while C_{AT} is a characteristic axial-torsional stiffness coupling term, which can be regarded as a direct consequence of the helicoidal geometry of the wire centerlines. The expressions of the axial and torsional stiffness terms are fully detailed in Appendix A.

From equation (31) the bending problem, under the full-slip kinematic assumption, turns out to be fully uncoupled from the axial-torsional one, and the flexural stiffness attains its minimum theoretical value $EI_{\min}$, which can be easily evaluated by considering all wires as individually bent. Accordingly, the following expression is obtained:

$$EI_{\min} = \sum_{j=0}^{\mathrm{m}} \frac{n_j}{2} \cos(\alpha_j) EI_{w,j} \left[1 + \cos^2(\alpha_j) + \frac{\sin(\alpha_j)}{1+\nu_j} \right] \tag{32}$$

On the other hand, the additional contribution $\mathbf{K}_{s,add}$ is non-symmetric and can be written in the following form:

$$\mathbf{K}_{s,add} = \begin{pmatrix} & k_{13} & k_{23} \\ \mathbf{0}_{2\times 2} & k_{14} & k_{24} \\ & k_{33} & 0 \\ \mathbf{0}_{2\times 2} & 0 & k_{44} \end{pmatrix} \tag{33}$$

The lacking of symmetry of the tangent stiffness matrix is consistent with the non-holonomic nature of the strand kinematic model adopted in this work. Indeed, an elastic potential function relating the strand generalized stress and strain variables could be defined only under one of the limit kinematic hypotheses of stick- or slip-state, as it has been extensively discussed by the authors with reference to a case of planar bending (Foti and Martinelli, 2016). More in details, at a given instant of the analysis, the

out-of-diagonal terms in (33) are strictly equal to zero if the distribution of wires in sticking state is circular symmetric with respect to the strand axis. This can be easily appreciated by analyzing e.g. the term k_{13} (analogous expressions hold for the other out-of-diagonal terms, as reported in Appendix B):

$$k_{13} = \frac{\partial N_s}{\partial \chi_{s2}} = \sum_{j=1}^{m} \sum_{i=1}^{n_j} k_{13,ij} \text{with} : k_{13,ij} = \begin{cases} \text{sticking} : \cos^3(\alpha_j) EA_{w,j} R_j \sin(\theta_i) \\ \text{slipping} : 0 \end{cases} \tag{34}$$

For circular symmetric distributions of wires in sticking, indeed, the sum $\sum_{i=1}^{n_j} \sin(\theta_i)$ is strictly equal to zero for any layer.

The stick-slip criterion defined by the interwire contact model adopted in this work can lead sometimes to non-symmetric distributions of wires in sticking state. However, both preliminary numerical tests (Foti, 2013) as well as theoretical results for a planar bending case (Foti and Martinelli, 2016), indicate that the effects of the out-of-diagonal terms in (33) can be neglected without affecting significantly the performances of the strand finite element formulation. The following symmetric approximation, hence, has been adopted in the present work:

$$\mathbf{K}_{s,add} \approx \begin{pmatrix} \mathbf{0}_{2\times 2} & \mathbf{0}_{2\times 2} \\ \mathbf{0}_{2\times 2} & \begin{matrix} k_{33} & 0 \\ 0 & k_{44} \end{matrix} \end{pmatrix} \tag{35}$$

The additional contributions to the direct stiffness terms are defined, respectively, as:

$$k_{ll} = \frac{\partial M_{sl}}{\partial \chi_{sl}} = \sum_{j=1}^{m} \sum_{i=1}^{n_j} k_{ll,ij} \text{with} : k_{ll,ij} = \left\{ \text{sticking} : \cos^3(\alpha_j) EA_{w,j} R_j^2 f_l(\theta_i) ; \text{slipping} : 0 \right\} \tag{36}$$

with: $l = 3,4$, $f_3(\theta_i) = \sin^2(\theta_i)$ and $f_4(\theta_i) = \cos^2(\theta_i)$.

It's worth noting that both terms, k_{33} and k_{44}, vary between zero and the maximum value $\sum_{j=1}^{m} \frac{n_j}{2} \cos^3(\alpha_j) EA_{w,j} R_j^2$, corresponding to the slip- and stick-state limit kinematic

assumptions, respectively. Therefore, the direct bending stiffness of the strand ranges between the minimum value $EI_{\min}$, defined in equation (32), and the maximum value:

$$EI_{\max} = EI_{\min} + \sum_{j=1}^{m} \frac{n_j}{2} \cos^3(\alpha_j) EA_{w,j} R_j^2 \tag{37}$$

7. Contact model

Interactions among adjacent wires occur at internal contact surfaces. Here friction forces tend to contrast relative interwire displacements, allowing for the transmission of tangential stresses between contacting wires. When the forces which tend to activate the sliding are greater than the frictional ones, then, a wire can undergo to relative displacements with respect to the neighbours.

Two basic contact conditions can be distinguished: *lateral* (or *circumferential*) contact, between wires belonging to the same layer (see Figure 2(a)); and *radial* contact, between wires in adjacent layers (see Figure 2(b)).

The geometric conditions for the occurrence of lateral contact have been analyzed by several authors (e.g.: Costello, 1990, Feyrer, 2007, Rawlins, 2005) with reference to the ideal case of a straight strand without imperfections. In this case the friction forces tend to contrast the onset of relative intra-layer displacements (*intra-layer sliding*). The contact takes place along continuous lines and the normal forces on the contacting surfaces are hoop actions, depending only on the geometry and the stresses of the layer components.

However, it's worth noting that typical strand constructions allow for interlayer clearances (Rawlins, 2005, Feyrer, 2007). Moreover, even if the theoretical geometrical conditions for lateral contact are satisfied, intra-layer gaps can be generated by manufacturing imperfections and strand ageing (Cardou and Jolicoeur, 1997) or by the loading process of the strand (Huang, 1978).

Taking into account the above remarks, the effects of lateral contact are neglected and a purely radial contact model is adopted in this work. Each wire, hence, is assumed in contact with those of the adjacent layers (interior and/or exterior) and the friction forces contrast relative inter-layer displacements (*inter-layer sliding*). Inter-

layer contact surfaces are, in general, pointwise distributed along helical paths (e.g. LeClair, 1991) which will be referred in the following as contact helices. The wires of the innermost layer make an exception, being in contact with the core wire along a continuous helix. By neglecting changes in the internal geometry of the strand with respect to its reference configuration, the contact helices of a generic wire with the internal and external layers are characterized by the same pitch of the wire centerline and helix radii equal to, respectively, $R^{int} = R - d/2$ and $R^{ext} = R + d/2$, where d denotes the wire diameter.

The following simplyfying assumptions are then introduced, according to (Papailiou, 1997, Hong, 2005), to analyze the radial contact conditions: (a) contact surfaces are assumed as not deformable and the discrete set of contact points is approximated with a continuous line (linear contact model); (b) a system of radial and tangential forces per unit length is introduced, on each contact helix, to model the interaction between wires; and (c) friction is described according to the classic Amontons-Coulomb model.

7.1. Sliding condition

Let's consider an infinitesimal wire segment dS, subjected to a system of distributed radial and tangential contact forces acting on the internal and external contact helices as it is schematically depicted in Figure 3. The equilibrium equations of the wire can be easily derived under the following simplyfying assumptions: (1) differences between the tangent vector of the wire centerline and those of the contact helices are neglected; (2) the distributed moments arising from the offset between the wire centerline and the application points of the tangential contact forces are neglected; (3) the contribution of the wire shear forces is neglected. Consequently, the system of equations (13) reduces to the equilibrium equations in tangential and radial direction, here rewritten as:

$$\frac{\partial F_{w1}}{\partial S} - c^{ext} f_t^{ext} - c^{int} f_t^{int} = 0; \;\; F_{w1}(S,t)\,\kappa + c^{ext} f_r^{ext} - c^{int} f_r^{int} = 0 \qquad \text{(38a, b)}$$

where: κ is the initial curvature of the wire centerline, defined in equation (8a), while c^{int} and c^{ext} are two non-dimensional coefficients, defined respectively as $c^{int} = 1 -$

$(\kappa d)/2$ and $c^{ext} = 1 + (\kappa d)/2$, which account for the difference between dS and the length of the infinitesimal segments of the contact helices.

The critical conditions for the onset of wire sliding, then, can be studied by assuming that the tangential forces per unit length satisfy the Amontons-Coulomb inequalities: $f_t^{ext} \leq \mu^{ext} f_r^{ext}$ and $f_t^{int} \leq \mu^{int} f_r^{int}$, where μ^{ext} and μ^{int} denote the friction coefficient of the external and internal contact surfaces. Hence, from equations (38a, b) and accounting also for a possible reversal in the direction of the wire axial force gradient, the following tangential contact condition is obtained:

$$\Psi(S,t) = \left| \frac{\partial F_{w1}}{\partial S} \right| - \mu^{int} F_{w1}(S,t)\,\kappa - \left(\mu^{ext} + \mu^{int}\right) c^{ext} f_r^{ext} \leq 0 \tag{39}$$

The function $\Psi(S,t)$ define the domain of admissible values of the wire axial forces, at a generic coordinate S. When $\Psi(S,t) < 0$ the tangential contact forces are large enough to prevent sliding, the wire is in the stick-state and behaves as a part of an ideal planar strand section. On the other hand, during the sliding of the wire the equality $\Psi(S,t) = 0$ must be strictly satisfied. As a consequence, the sliding conditions can be expressed in the following rate form:

$$\begin{cases} \Psi(S,t) = 0 \\ \dot{\Psi}(S,t) = 0 \end{cases} \tag{40}$$

It can be noticed, from equation (39), that the function $\Psi(S,t)$ in general depends on the radial contact forces f_r^{ext}, on the axial force in the wire, $F_{w1}(S,t)$, and on the past history of the wire.

At a given time t, the radial forces acting on the wire can be evaluated by imposing the equilibrium in radial direction through a recursive procedure, which starts at the outermost layer and moves towards the core of the strand. Within this context, it's possible to show that the function $F_{w1}(S,t)$ is the only unknown in equation (39), which can be also re-written, formally, as:

$$\Psi(S,t) = \left| \frac{\partial F_{w1}}{\partial S} \right| - g\left(F_{w1}(S,t)\right) \leq 0 \tag{41}$$

where $g(\cdot)$ is a function of the wire axial force only.

7.2. Evaluation of the radial contact forces

In the following, a new, concise, formulation will be presented that will use product notation to express the radial contact forces. As a further novelty, the results we present allow to account for the residual radial contact forces due to the manufacturing process of the strand. This last point can have an important role in controlling the stiffness and the energy dissipation at low values of axial force.

The radial contact conditions can be studied starting from the literature assumption (see e.g.: Lanteigne, 1985; Papailiou, 1997; Rawlins, 2009), that all wires in a layer are subjected to the same external radial contact forces. Hence, the equilibrium in the radial direction at the interface between two generic layers, j and $j-1$, requires that:

$$n_j f_{r,j}^{int} = n_{j-1} f_{r,j-1}^{ext} \tag{42}$$

where the symbol n_k denotes the number of wires in the k^{th} layer.

The radial equilibrium equation of a wire (38b), then, can be iteratively solved together with the condition (42) starting from the outermost layer (layer m), where the external radial forces are assumed equal to zero (unloaded strand lateral surface). The following recursive expressions can be obtained:

$$f_{r,j}^{ext} = \frac{1}{n_j} \sum_{l=j+1}^{m} \Gamma(l,j)\, \beta_l F_{w1,l}^{av};\;\; f_{r,j}^{int} = \frac{1}{n_j} \beta_j F_{w1,j}^{av} + \gamma_j f_{r,j}^{ext} \tag{43a, b}$$

where $F_{w1,j}^{av}$ is the average axial force of the wires in the j^{th} layer, i.e.: $F_{w1,j}^{av} = \frac{1}{n_j} \sum_{i=1}^{n_j} F_{w1,ij}$ and $\Gamma(l,j)$ is a function defined as: $\Gamma(l,j) = \prod_{k=j+1}^{l-1} \gamma_k$.

Coefficients β_j and γ_j , which appear in the above equations, depend only on the geometric characteristics of the j^{th} layer through the non-dimensional coefficients c_j^{int} and c_j^{ext} (see Section 7.1) and the initial curvature of the wire centerline κ_j (see equation (8a)):

$$\beta_j = \frac{n_j \kappa_j}{c_j^{int}};\;\; \gamma_j = \frac{c_j^{ext}}{c_j^{int}} \tag{44a, b}$$

As it can be easily inferred from equations (43a, b), the analysis above neglects the effects on the radial contact conditions of the residual stresses due to the manufacturing process.

In fact, the stranding process determines a complex stress-strain state, involving plastic strains of the wires and residual, self-equilibrated, three-dimensional stresses (see e.g. Webster and Mills, 1998). Residual radial forces (Rawlins, 2005), which are represented in Figure 4 for a generic component of the outermost layer of the strand, act on the internal contact helix and tend to force the wire away from the strand axis, concurring to the typical radial springback effect when the strand is cut.

The effect of the residual radial contact forces, R_j, acting on the generic j^{th} layer, can be accounted for by slightly modifying the recursive expressions (43a, b), respectively, as it follows:

$$\begin{aligned} f_{r,j}^{ext} &= \frac{1}{n_j} \sum_{l=j+1}^{m} \Gamma(l,j)\, \beta_l F_{w1,l}^{av} + \frac{1}{n_j} \sum_{l=j+1}^{m} \Gamma(l,j)\, n_l R_l \\ f_{r,j}^{int} &= \frac{1}{n_j} \beta_j F_{w1,j}^{av} + \gamma_j f_{r,j}^{ext} + R_j + \frac{1}{n_j} \sum_{l=j+1}^{m} \Gamma(l,j)\, n_l R_l \end{aligned} \qquad \text{(45a, b)}$$

As it can be easily observed from the above equations, the effect of the residual stresses on the overall radial contact forces increases with the decreasing of the wire axial forces created by the external loads acting on the strand.

7.3. Solution algorithm

The proposed contact model can be used within the framework of an incremental analysis to evaluate whether a generic section of a wire is undergoing to sliding (*slipping-state*), or not (*sticking-state*). The state evaluation is performed through a Return Map Algorithm, based on a sticking-state prediction and slipping-state correction. As a result, the value of the gradient of the axial force is obtained. From this, the axial force $F_{w1}(S,t)$ can be evaluated along the wire through standard numerical integration techniques.

It's worth noting that in the formulation herein proposed, the difference between sticking or slipping states is essentially due to the kinematic assumptions made in Section 5 about the generalized wire strains. In fact, once these have been evaluated (ac-

cording to a sticking or slipping state assumption), the wire and strand stress resultants can be easily evaluated through the elastic model outlined in Sections 4 and 6.

The Return Map Algorithm delivers the values of the axial force gradient at a discrete number of cross sections along the wire. The wire axial force $F_{w1}(S,t)$, then, can be numerically evaluated starting from suitable boundary conditions. These are specified in this work for the special case of an infinite strand subjected to a strain state variable in time, but uniform along its length. This is a very interesting and important case since it allows to define cross sectional moment-curvature relations which can be considered as representative of the strand behaviour sufficiently far away from the constraints, or from concentrated loads.

Under the hypothesis of uniform strains of the strand, the solution of the axial-torsional problem gives uniform axial strain along the wires (see Eq. (15)). By recalling that wires are assumed as linearly elastic, it can hence be concluded that the gradient of the wire axial force depends on the bending contributions only.

Let's first consider the case of uniform monotonic bending. At the beginning of the analysis, the wires satisfy the stick state kinematic assumption and their axial force can be evaluated from equations (12) and (16). Accordingly, the wire axial force due to bending turns out to be a sinusoidal function of the swept angle θ , equal to zero where the wire crosses a plane perpendicular to the plane of bending, which in the following will be referred to as the neutral plane of bending, with a slight abuse in terminology. At the same points, for geometrical reasons, the axial force gradient attains its maximum absolute values and, as a consequence, the wire cross sections are more prone to slide.

Coherently with these observations, classic literature models (e.g.: Papailiou, 1997, Hong et al., 2005) assume that the bending contribution to the wire axial force is equal to zero at the sections where the wire crosses the neutral plane of bending, where the wire slipping starts. This hypothesis, which allows to write simple periodic boundary conditions for the wire axial force (see also Foti and Martinelli, 2016), has been adopted also in the present work within the more general framework of an incremental analysis.

To further clarify the main features of the proposed approach, let's consider the bending of a single layer strand (see Figure 5), which will be further considered for numerical applications in Section 8.1. The strand is composed by six wires wound

around a straight core (1/6 steel strand). The geometric and material properties of the strand are summarized in Table 1 while the friction coefficient is assumed as $\mu = 0.5$. The strand is assumed subjected to a constant axial force, equal to the 10% of its Ultimate Tensile Strength (UTS), experimentally determined by Utting and Jones (1987a) as 137 kN. For simplicity, the effects of the residual contact forces due to the stranding process are for now neglected.

A monotonic bending process in the plane (x_1, x_3) is then considered (see Figure 5(a)). Figure 6(a) shows the axial force along an external wire (*wire 1* in Figure 5(b)) of the strand. The solution has been numerically evaluated by using 72 integration points over the pitch of the helicoidal wire centerline to solve the proposed contact model. Due to the periodic character of the solution, only the interval $\theta \in [0, 2\pi]$ of the swept angle is plotted.

As it can be easily appreciated from Figure 6(a), by increasing the curvature of the strand the response of the strand moves from a linear-elastic sinusoidal solution (see e.g. the curves related to the curvatures χ_A and χ_B) toward a *limit solution* which is associated to the sliding of the whole pitch of the wire. In this special case (namely: single strand, combination of axial load and simple bending) the limit solution approached by the proposed model for large values of curvature, substantially coincides with the analytical expression proposed by Papailiou (1997). The more refined proposed model leads nevertheless a) to about a 15% difference on the maximum value, and b) to a curve that is C^1 continuous instead of one that is only C^0.

Once the axial force in the external wires of the strand is known, it's also possible to evaluate the cross sectional bending moment through the procedure detailed in Section 6.1. The moment-curvature curve evaluated by considering a different number of integration points along a generic external wire is shown in Figure 6(b). Solutions obtained with 18, 36 and 72 points are practically coincident, showing a fast convergence of the numerical procedure.

8. Numerical validation and applications

The strand mechanical model has been implemented within a three-dimensional (3-D) corotational beam finite element, to perform large scale structural analyses. The finite element formulation here adopted has been originally developed by one of the authors (Foti, 2013), and it's explicitly conceived (Foti et al., 2015) to perform static and dynamic analyses for flexible structures, undergoing large displacements and rotations, but small strains.

In the following the performance of the proposed formulation and finite element implentation will be assessed first for combined axial-torsional loading, with respect to a single-layer strand, and subsequently for bending, specially focusing on the role of the residual contact forces due to the stranding process. Reference will be made to well-documented physical tests and established analytical formulations.

8.1. Axial-torsional coupling problems

As an initial validation of the proposed formulation the axial-torsional response of a single-layer strand is studied with reference to a well-documented benchmark (see e.g.: Utting and Jones, 1987b; Jiang et al. 1999; Judge, 2012) for which experimental data are available (Utting and Jones, 1987a). The geometric and material properties adopted for the strand are listed in Table 1. During the original testing, the strand has been subjected to a combination of axial force and torsional moment applied at the end sections in the straight configuration. To this aim, a tension-torsion machine was used (Utting and Jones 1987a). The machine applies a prescribed axial elongation to the strand, while the corresponding axial force is recorded. One end of the strand is fully clamped, while the other can be free (free-end case) or fully restrained (fixed-end case). In the latter case, the reacting torsional moment is recorded. This is a standard setup for tensile testing of metallic strands (Feyrer, 2007), which allows to reproduce the theoretical condition of uniform stress-strain state along the element.

Numerical simulations have been carried out according to the formulation proposed in the present work. Radial contact conditions have been considered to calculate the helix radius of the wires. The specimen was simulated with a one meter long stretch

of strand, using ten equally spaced corotational beam elements. One end of the strand has been considered fixed, and a prescribed axial displacement has been imposed at the other end section, where free or fully restrained torsional rotations have been considered in order to reproduce the different test conditions.

The results from the proposed model will also be assessed, for comparison purposes, against the well-known Costello's theory (Costello, 1990). Differently from the approach proposed in the present work, the Costello's analytic formulation accounts for the contraction of wire radius due to the Poisson effect and the related changes of the strand internal structure, and the resulting model, which is then slightly non-linear (geometric nonlinearity), is at the base of the solutions presented by Jiang et al. (1999) that will be reported here.

The response of the strand is shown in Figure 7. Excellent agreement is found in the whole linear range of the response between the proposed model, the experimental results and Costello's theory. Since both the proposed model and Costello's one are based on the hypothesis of linearly elastic material behaviour they fail to reproduce the plastic phenomena which precede the breaking of the strand.

The direct axial stiffness, $k_1 = N_s/\varepsilon_s$, and the coupling coefficient, $k_2 = N_s/M_s$, predicted by both models are compared in Table 2 with the experimental values measured in the elastic range of the response. It can be observed how the discrepancies between the proposed model and the experimental results are always less than 3%. Furthermore, the proposed model and the Costello's theory show similar accuracy in predicting the stiffness k_1, both for the fixed- as well as for the free-end case.

The Costello's model, instead, shows a slightly greater accuracy in predicting the coupling term k_2. This could be due to the fact that, accounting for the contraction of the wire diameters due to the Poisson effect, the Costello's model delivers a better estimation of the helix radius of the external wires under loading conditions. This geometric parameter, in turns, tends to affect the coupling term k_2 more than the direct axial stiffness k_1, as it can be also inferred by analysing the axial-torsional stiffness coefficients of the proposed model given in Appendix A.

The results obtained with the proposed cross sectional and finite element formulations are noteworthy for their accuracy with respect both to experimental tests and

established analytical theories. This aspect is of high interest since it allows for their use with confidence in the study of more complex problems, and large scale structural analyses, for which obtaining an analytical solution would become increasingly complex.

8.2. Bending problems

8.2.1. Cross sectional behaviour

The bending behaviour of a four-layer stranded electrical conductor (ACSR Curlew 7/54) is investigated in this section. This is a very interesting case since Rawlins (2005) has provided a calculation of the residual contact forces due to the stranding process. This case can then be exploited to assess the role of this aspect on the bending behaviour of a typical multi-layer strand within the formulation proposed in the present paper.

The cable at study is made of seven steel wires surrounded by fifty-four aluminium wires, grouped in three concentric layers according to a reverse lay construction. The geometric and material properties of the strand are listed in Table 3, along with the residual contact forces given by Rawlins (2005) for the specific manufacturing process.

Figure 8 shows a typical moment-curvature hysteresis loop, computed with the proposed model by applying a cyclic curvature, with limits $\pm\chi_{\max}$, to the strand cross section. The first loading branch is characterized by the initial stiffness $EI_{\max}$, corresponding to the full-stick state. The tangent stiffness, then, gradually decreases as a consequence of the evolution of the interwire sliding phenomena. Note that it is assumed that $\pm\chi_{\max}$ is sufficiently large to achieve the limit value $EI_{\min}$, which can be attained only if all wires of the cross section are in the slipping state. The ratio between the maximum moment reached and the associated curvature $\chi_{\max}$ is used to define the secant stiffness of the cycle: EI_{sec}.

In order to compare different hysteresis loops, the area enclosed within a full loop is denoted as A_{cycle}. This is a very important physical parameter, related to the energy dissipated in bending per unit of length during vibrations of the cable. Moreover, to quantitatively characterize the shape of the first loading branch, the parameters χ_0 and M_0 are introduced as shown in Figure 8. They define the coordinates of the yielding point of an "ideal" bi-linear elastic-plastic moment-curvature relation.

To assess the proposed modelling approach, and the effect of the main physical parameters, numerical tests have been carried out for: (a) a broad range of tensile loads, identified through the ratio η between the axial force and the ultimate tensile strength of the strand, and (b) different values of the interwire friction coefficient, μ. The latter has been considered the same for all internal contact surfaces, and ranging between the values $0.3 \leq \mu \leq 0.7$ in order to cover the whole interval of values typically adopted in literature (e.g. Papailiou, 1997; Hong, 2005). All simulations have been carried out both considering, as well as neglecting, the residual contact forces in order to systematically assess their role on the strand response.

Firstly, the effects of the axial force on the bending behaviour of the strand will be discussed (e.g. see Figure 9). To this end, the friction coefficient is assumed equal to $\mu = 0.7$, while the load parameter η is varied within the range: $0 \leq \eta \leq 0.5$. It's worth noting that this range of values represents many different structural conditions, which can be broadly classified as: "slack" $(\eta < 0.1)$, "moderately taut" $(0.1 \leq \eta < 0.3)$ and "taut" cables $(\eta \geq 0.3)$. Suspended cables of overhead electric lines, where ACSR conductors are used, typically belong to the range of "moderately taut" cables (see e.g. Orawski, 2003).

Figure 9 shows the first loading branch of the moment-curvature curves for three different values of η in the moderately taut range. The curves have been evaluated both considering (Figure 9(a)) as well as neglecting (Figure 9(b)) the residual radial contact forces. In both cases, the effects of the tensile load are qualitatively the same. In particular, by increasing η the nonlinear transition region between the initial full-stick behaviour (initial stiffness: $EI_{\max}$) and the full-slip regime (constant tangent stiffness: $EI_{\min}$) is expanded. In fact, by increasing the axial load, the radial contact forces between the wires are also increased and higher values of the wire axial force gradient are needed to activate the sliding. The axial force gradient, in turn, is controlled by the bending curvature. Hence, by increasing the axial load, higher curvatures are needed to activate the sliding of wires. Within this context, the residual contact forces can give a significant contribution to prevent interwire sliding, as it can be easily appreciated by comparing Figures 9(a) and 9(b).

A deeper insight, can be gained by considering the variation of the parameters χ_0

and M_0 with η, which is depicted in Figure 10. Both parameters vary linearly and the residual contact forces determine a rigid translation of both functions $\chi_0(\eta)$ and $M_0(\eta)$ along the ordinate axes. Figure 11 shows as a function of η the difference (symbol Δ) between the values of χ_0 and M_0 evaluated considering or not the residual contact forces. Accordingly, the relative error which can be introduced in the evaluation of χ_0 and M_0 by neglecting the effect of the residual contact forces varies largely as a function of η. By increasing the axial load of the strand, indeed, the relative contribution of the residual contact forces to the total ones is reduced. In particular, the difference ranges between 100% and 25% for slack cables; between 25% and 10% for moderately taut cables; and between 10% and 6% for taut cables, using the residual forces of the case at study.

These results clearly highlight the importance of the residual contact forces on the modelling of slack cables undergoing flexural vibrations. This is a very important finding also for the analytical and numerical modelling of a number of mechanical components that adopt slack wire ropes as a source of damping, such as Stockbridge dampers for the control of cable aeolian vibrations (e.g. Sauter and Hagedorn, 2002; Foti and Martinelli, 2013) or as isolation devices (Gerges, 2008). Furthermore, the residual contact forces can also significantly affect the cross sectional response of moderately slack cables, such as those employed in electrical overhead conductors.

As per the friction coefficient μ, its variation leads to effects that are qualitatively similar to those of a variation the strand axial force. Figure 12 shows the first loading branch of the moment-curvature curves for a moderately taut strand $(\eta = 0.15)$ and three different values of the friction coefficient. At an increase of μ, also the curvature needed to activate the interwire sliding increases. As a consequence, the transition between the full-stick and the full-slip regions is also increased. The presence of a residual contact force due to the rope formation process doesn't affect this qualitative behaviour, even if appreciable differences can be noticed from a quantitative point of view (in the order of $20\% - 25\%$ for parameter M_0). In Figure 13 the parameters χ_0 and M_0 are plotted as a function of the friction coefficient for three different values of η, which can be considered representative of slack $(\eta = 0.01)$, moderately taut $(\eta = 0.15)$ and taut $(\eta = 0.40)$ cables. The variation of these parameters is almost

linear with the friction coefficient, both when residual contact forces are considered or not. Moreover, it can be noticed that the slope of the curves $\chi_0(\eta)$ and $M_0(\eta)$ increases with increasing values of μ. Hence, it can be concluded that the effects of a variation of the friction coefficient are greater for increasing values of the strand axial force.

Finally, the hysteretic behaviour of the strand cross sections was investigated for different values of the maximum bending curvature $\chi_{\max}$. As expected from the results previously presented with reference to the first loading branch, the shape of the loops is not affected from a qualitative viewpoint by the presence of residual contact forces, which, however, clearly affect the size of the moment-curvature cycles.

In order to gain a deeper insight on the effects of the residual contact forces on the cyclic bending of the strand, the area enclosed in the loops and the secant stiffness have been evaluated for different values of $\chi_{\max}$ and for two different values of η: 0.15 and 0.40, which, as already mentioned, represent moderately taut and taut cables.

Accordingly with the fact that residual contact forces don't affect the shape of the hysteresis loops, the secant stiffness of the loops is not affected by the residual contact forces, as it can be inferred from Figure 14(b), where the non-dimensional stiffness ratio $EI_{\text{sec}}/EI_{\max}$ is plotted against the ratio between the maximum curvature $\chi_{\max}$ and the parameter χ_0. As expected, the non-dimensional secant stiffness continuously decreases with increasing values of the maximum curvatures, tending to the limit theoretical value of $EI_{\min}/EI_{\max}$ for infinite curvature $\chi_{\max}$.

The area of the loops, on the other hand, can be strongly affected by the residual contact forces, as it can be appreciated from Figure 14(a). The relative difference between the area evaluated with or without contact forces, denoted as ΔA_{cycle}, is plotted in Figure 15 against the ratio $\chi_{\max}/\chi_0$. It can be observed that ΔA_{cycle} is almost constant with respect to $\chi_{\max}/\chi_0$ and increases with decreasing values of the strand axial force. The results depicted in Figure 15 also point out that neglecting residual contact forces can lead to a significant underestimate of the hysteresis loop area both for moderately taut (about 40% for $\eta = 0.15$) as well as for taut (about 20% for $\eta = 0.40$) cables. This finding can be especially important for the modelling of the self-damping of strands undergoing flexural vibrations.

8.2.2. Element behaviour

The proposed formulation, and the corotational finite element implementation, are in this section applied to model the quasi-static non-linear bending behaviour of an axially unloaded multi-layer steel strand. A "Galfan coated" steel strand is considered. The element has outer diameter equal to 38 mm (Galfan $\phi 38$), and is made of 37 wires, grouped in four concentric layers with reverse lay construction. The numerical predictions are compared with recent experimental results (Chen et al., 2015) to show the effectiveness of the proposed formulation in reproducing both the qualitative as well as the quantitative features of the strand bending response.

The tests, fully described in (Chen et al., 2015), were carried out by applying a quasi-static concentrated vertical load, V, at the midspan of a simply supported and axially unloaded specimen. A schematic representation of the experimental test setup is shown in Figure 16. The total length of the specimen is equal to 1050 mm, while the distance between the supports is equal to 820 mm, this assures a significant bending response for the diameter of the strand. Both supports are specifically designed to allow free-end torsional rotations of the strand cross section.

Numerical analyses have been carried out with the proposed formulation to simulate the experimental tests. A mesh of 32 equally spaced corotational beam finite elements has been adopted to represent the portion of the strand between the supports. Mesh refinements have been also considered in preliminary calculations to check the accuracy of the numerical model. The geometric and material parameters of the strand model have been defined as it follows. The helix radii of the wires have been evaluated by imposing the radial contact condition between adjacent layers and the lay angles have been assumed equal to the characteristic values of 6° for the innermost layer and 14° for the remaining layers. The Young modulus and the Poisson coefficient of steel have been assumed equal to, respectively, $E = 200$ GPa and $\nu = 0.3$.

The analyses have been carried out by considering different values of the friction coefficient, μ, and of the radial residual contact force, R. Both parameters have been considered constant for all layers and varying within a range of value characteristic for steel strands.

Figure 17 shows a comparison between the experimental and numerical load-displacement curves of the structure. The experimental response of the structure (depicted with dots in Figure 17) is initially characterized by the maximum value of the tangent stiffness and almost linear. By increasing the value of the applied vertical load the stiffness of the structure decreases, until a minimum constant value is attained.

Very good agreement is found between the experimental data and the numerical solutions. Both the initial (maximum) as well as the final (minimum) tangent stiffness of the structure are predicted with reasonable accuracy (8% error on the initial stiffness and 14% on the final one). Furthermore, the non-linear evolution of the response is well captured both from a qualitative as well as from a quantitative point of view. In Figure 18 the related distribution of the wires in slip-state is reported for the section at the mid span in the loading range $V = 200 - 460$ N. As it can be noted, the first wires to slip are the ones closer to the neutral axis in the outermost layer, then the wires further away. This slipping pattern is repeated from the outermost layer to the internal ones.

The simulations presented in Figure 17(a) have been carried out for a friction coefficient $\mu = 0.7$ and different values of the residual contact force, R. The effect of a variation of the friction coefficient, instead, can be appreciated from Figure 17(b), where the results obtained for $R = 4$ N/mm and three different values of μ are shown. Within this context, the best match between experimental data and numerical results is obtained for the set of parameters: $\mu = 0.7$ and $R = 4$ N/mm. Furthermore, it should also be noted that, should the radial residual contact force R be assumed equal to zero, as to the knowledge of the authors it is implicitly done in all literature models available to date, the curves described by the straight lines labelled $EI_{\min}$ would be have been obtained in Figure 17. This would have lead to wholly not capturing the experimental evidence and to an unacceptable error also with respect to the initial bending stiffness.

These results, once more, highlight the importance of the residual contact forces on the modelling of slack cables undergoing bending deformations.

9. Conclusions

In the present work a refined description of metallic strands, fully accounting for their nature of composite structural materials and the hysteretic bending behavior, is developed and is linked to a structural theory for large-scale analyses of three-dimensional cable structures undergoing large displacements and rotations. From the developments and the results offered in the previous Sections, the following conclusions and comments can be drawn.

A new sectional model is formulated and validated that, differently from most models currently available in the literature, takes into account the effects on the response due to the residual radial contact forces coming from the strand manufacturing process. This allows to avoid the common error of predicting a linearly elastic response for slack cables, which is in contrast with experimental findings.

Most of available models are confined to the case of planar flexural vibrations of tensioned strands, the one herein proposed has been casted in the form of a generalization to the biaxial bending of classic stick-slip kinematic relations for the planar bending of strands. Furthermore, a new procedure to compute the curvature of wires is presented, based on the assumption that the cross section of the wires rotates rigidly with the cross section of the strand.

The inherently non-linear problem of bending of the strand has been stated in rate form to make easier the adoption of the classic tools of non-holonomic material mechanics. Accordingly, a Return Map Algorithm has been proposed and validated for its solution within a nonlinear incremental structural analysis. The tangent operator has been studied and it was found that:

1. Under the assumption of linearly elastic behaviour of wires, the non-linearities in the cross section stiffness matrix are only due to the contribution of the wire axial strain induced by the bending of the strand.
2. Lacking of symmetry of the tangent stiffness matrix is consistent with the non-holonomic nature of the strand kinematic model adopted in this work. This is due to both the axial force, as well as the torsional moment, coupling with the bending curvatures.

3. The non symmetric coupling of the stiffness terms is strictly zero for circular symmetric distribution of wires in sticking-state, and can be neglected without affecting the numerical solution.

Under the assumptions of a radial linear contact and the Amontons-Coulomb friction law, a new concise formulation to express the radial contact forces has been presented in the form of product notation. The proposed contact model allows to:

1. Easily account for the residual radial contact forces due to the manufacturing process of the strand. As it has been pointed out through extensive numerical simulations, and by comparison with experimental results, this last point has an important role in controlling the stiffness and the energy dissipation at low values of axial force.
2. Obtain a C^1 continuous solution that, for large values of curvature, approaches (with a difference of about 15% on the maximum value) the C^0 proven analytical expressions for bending proposed by Papailiou (1997).

Furthermore, it was also found that the effect of the residual stresses on the overall radial contact forces increases with the decreasing of the wire axial forces created by the external loads acting on the strand.

The proposed cross sectional formulation has been implemented into a three-dimensional finite element formulation for corotational beams to perform static and dynamic analyses of flexible structures, undergoing large displacement and rotations. The performance of the proposed approach has been assessed, both for combined axial-torsional loading and for bending, with reference to well-documented physical tests and established analytical formulations. Special attention was devoted to the role of residual contact forces due to the stranding process. The axial-torsional response of a single-layer steel strand was reproduced with good accuracy. The bending behaviour was investigated with reference to a typical multi-layer stranded electrical conductor for which the residual contact forces due to the stranding process were known. The effect of the main physical parameters have been studied for a broad range of tensile loads and different values of the interwire friction coefficient.

While the value of residual radial contact forces doesn't change the main features of the monotonic moment-curvature response, it however heavily influences the reference value of the transition curvature (and corresponding bending moment) from the initial full-stick behaviour and the full-slip regime. In particular, a variation in the range between 100% and 25% for "slack" cables, and in between 25% and 10% for "moderately taut" cables was found using the residual forces of the case at study. The effects of the residual contact forces on the cyclic bending of strands can be similarly described. The residual contact forces don't affect the shape of the hysteresis loops but do strongly affect their area, with obvious implication on the self-damping modelling of structures and mechanical components that include slack or moderately taut wire ropes.

Finally, the study of the quasi-static non-linear bending behaviour of an axially unloaded multi-layer steel strand showed the effectiveness of the proposed formulation in reproducing both the qualitative, as well as the quantitative, features of the strand experimental bending response, emphasizing the importance of the residual forces. It should be noted, in fact, that by disregarding the radial residual contact forces, as it is implicitly done in common practice, a linearly elastic response would have been obtained not capturing the experimental evidence.

Appendix A. Evaluation of the axial-torsional cross sectional stiffness terms

By denoting as m the number of layers, n_j the number of wires belonging to the j^{th} layer, and reserving the subscript "0" to the quantities referred to the core wire, the axial and torsional cross sectional stiffness (see also equation (31)) terms can be expressed as it follows:

$$EA = \sum_{j=0}^{\mathrm{m}} n_j c^3(\alpha_j) EA_{w,j} \tag{A.1}$$

$$GJ = \sum_{j=0}^{\mathrm{m}} n_j \left\{ \frac{EI_{w,j}}{1+\nu_j} \left[c^3(\alpha_j) + (1+\nu_j) s^2(\alpha_j) c(\alpha_j) \right] + s^2(\alpha_j) c(\alpha_j) R_j^2 EA_{w,j} \right\} \tag{A.2}$$

$$C_{AT} = \sum_{j=0}^{\mathrm{m}} n_j R_j s(\alpha_j) c^2(\alpha_j) E A_{w,j} \tag{A.3}$$

where the symbols $s(\cdot)$ and $c(\cdot)$ shortly denote the sine and cosine functions, respectively.

Appendix B. Evaluation of the out-of-diagonal terms of the matrix $\mathbf{K}_{s,add}$

This appendix provides closed-form expressions for the out-of-diagonal terms of the additional contribution, $\mathbf{K}_{s,add}$, to the cross sectional tangent stiffness matrix (see equations (30) and (33)).

Under the assumption of axisymmetry of the strand, the following identities hold true:

$$\sum_{i=1}^{n_j} \sin(\theta_i) = \sum_{i=1}^{n_j} \cos(\theta_i) = \sum_{i=1}^{n_j} \sin(\theta_i)\cos(\theta_i) = 0 \tag{B.1}$$

where n_j is the number of wires belonging to the generic j^{th} layer.

By exploiting the relations above it can be easily shown that the only terms of $\mathbf{K}_{s,add}$ which are not identically equal to zero are: (a) k_{13} and k_{14}, which express the coupling between the strand axial force and the bending curvatures, and (b) k_{13} and k_{14}, which express the coupling between the strand torsional moment and the bending curvatures. The contribution of the individual wires to these stiffness terms depends on their kinematic state (i.e.: sticking- or slipping.-state). By denoting as m the number of

layers in the strand, the following expressions are obtained:

$$k_{13} = \frac{\partial N_s}{\partial \chi_{s2}} = \sum_{j=1}^{m} \sum_{i=1}^{n_j} k_{13,ij} \text{with} : k_{13,ij} = \begin{cases} \text{sticking} : \cos^3(\alpha_j) EA_{w,j} R_j \sin(\theta_i) \\ \text{slipping} : 0 \end{cases}$$

$$k_{14} = \frac{\partial N_s}{\partial \chi_{s3}} = \sum_{j=1}^{m} \sum_{i=1}^{n_j} k_{14,ij} \text{with} : k_{14,ij} = \begin{cases} \text{sticking} : \cos^3(\alpha_j) EA_{w,j} R_j \cos(\theta_i) \\ \text{slipping} : 0 \end{cases}$$

$$k_{23} = \frac{\partial M_{s1}}{\partial \chi_{s2}} = \sum_{j=1}^{m} \sum_{i=1}^{n_j} k_{23,ij} \text{with} : k_{23,ij} = \begin{cases} \text{sticking} : \sin(\alpha_j) \cos^2(\alpha_j) EA_{w,j} R_j^2 \sin(\theta_i) \\ \text{slipping} : 0 \end{cases}$$

$$k_{24} = \frac{\partial M_{s1}}{\partial \chi_{s3}} = \sum_{j=1}^{m} \sum_{i=1}^{n_j} k_{24,ij} \text{with} : k_{24,ij} = \begin{cases} \text{sticking} : \sin(\alpha_j) \cos^2(\alpha_j) EA_{w,j} R_j^2 \cos(\theta_i) \\ \text{slipping} : 0 \end{cases}$$

(B.2a, b, c, d)

It can be easily noticed that, according to the identities (B.1), all the coupling terms listed above are strictly equal to zero for circular symmetric distributions of the wires in sticking.

References

[1] (Cardou and Jolicoeur, 1997) A Cardou, C Jolicoeur, Mechanical models of helical strands, Applied Mechanics Review ASME 50, 1-14.

[2] (Cardou, 2006) A Cardou, Taut helical strength bending stiffness, www.utfscience.de I/2006, 2006.

[3] (Chen et al., 2015) Z Chen, Y Yu, X Wang, H Liu, Experimental research on bending performance of structural cable, Construction and Building Materials 96, 279-288, 2015.

[4] (Costello, 1990) GA Costello, *Theory of wire ropes*, Springer-Verlag, New York USA, 1990.

[5] (Dastous, 2005) JB Dastous, Nonlinear finite-element analysis of stranded conductors with variable bending stiffness using the tangent stiffness method, IEEE Transactions on Power Delivery 20, 328-338, 2005.

[6] (Feyrer, 2007) K Feyrer, *Wire ropes: tension, endurance, reliability*, Springer-Verlag, Berlin Heidelberg, 2007.

[7] (Foti, 2013) F Foti, *A corotational beam element and a refined mechanical model for the nonlinear dynamic analysis of cables*, Doctoral Dissertation, Politecnico di Milano, Milan (Italy), 2013.

[8] (Foti and Martinelli, 2013) F Foti, L Martinelli, Modeling of the hysteretic dynamic behavior of the Stockbridge messenger cables, Proocedings of the XXI Conference of the Italian association of Theoretical and Applied Mechanics AIMETA, Torino (Italy), 2013.

[9] (Foti and Martinelli, 2016) F Foti, L Martinelli, An analytical approach to model the hysteretic bending behavior of spiral strands, Applied Mathematical Modelling, In press. (http://dx.doi.org/10.1016/j.apm.2016.01.063)

[10] (Foti et al., 2015) F Foti, L Martinelli, F Perotti, Numerical integration of the equations of motion of structural systems undergoing large 3D rotations: dynamics of corotational slender beam elements, Meccanica 50, 751-765, 2015.

[11] (Gerges, 2008) RR Gerges, Model for the force-displacement relationship of wire rope springs, Journal of Aerospace Engineering ASCE 21, 1-9, 2008.

[12] (Giglio and Manes, 2003) M Giglio, A Manes, Bending fatigue on a metallic wire rope for aircraft rescue hoist, Engineering Failure Analysis 10, 223-235, 2003.

[13] (Goudreau et al., 1998) S Goudreau, F Charette, C Hardy, L Cloutier, Bending Energy Dissipation of Simplified Single-Layer Stranded Cable, Journal of Engineering Mechanics ASCE 124, 811-817, 1998.

[14] (Hong et al., 2005) KJ Hong, A Der Kiureghian, JL Sackman, Bending behavior of helically wrapped cables, Journal of Engineering Mechanics ASCE 131, 500-511, 2005.

[15] (Huang, 1973) NC Huang, Theories of Elastic Slender Curved Rods, Journal of Applied Mathematics and Physics (ZAMP) 24, 1-19, 1973.

[16] (Huang, 1978) NC Huang, Finite Extension of an Elastic Strand With a Central Core, Journal of Applied Mechanics ASME 45, 852-859, 1978.

[17] (Inagaki et al., 2007) K Inagaki, J Ekh, S Zahrai, Mechanical analysis of second order helical structure in electrical cable, International Journal of Solids and Structures 44, 1657-1679, 2007.

[18] (Irvine, 1981) HM Irvine, *Cable Structures*, The MIT Press, Cambridge USA, 1981.

[19] (Jiang et al., 1999) WG Jiang, MS Yao, JM Walton, A concise finite element model for simple straight wire rope strand, International Journal of Mechanical Sciences 41, 143-161, 1999.

[20] (Judge et al., 2012) R Judge, Z Yang, SW Jones, G Beattie, Full 3D finite element modelling of spiral strand cables, Construction and Building Materials 35, 452-459, 2012.

[21] (Kreyszig, 1991) E Kreyszig, *Differential geometry*, Dover Publications, New York USA, 1991.

[22] (Lacarbonara and Pacitti, 2008) W Lacarbonara, A Pacitti, Nonlinear modelling of cables with flexural stiffness, Mathematical Problems in Engineering, ID 370767, 1-21, 2008.

[23] (Langlois et al., 2014) S Langlois, F Légeron, F Levesque, Time history modeling of vibrations on overhead conductors with variable bending stiffness, IEEE Transactions on Power Delivery 29, 607-614, 2014.

[24] (Lanteigne, 1985) J Lanteigne, Theoretical estimation of the response of helically armoured cables to tension, torsion and bending, Journal of Applied Mechanics ASME 52, 423-432, 1985.

[25] (LeClair, 1991) RA LeClair, Axial response of multilayered strands with compliant layers, Journal of Engineering Mechanics ASCE 117, 2884-2903, 1991.

[26] (Lee, 1991) WK Lee, An insight into wire rope geometry, International Journal of Solids and Structures 28, 471 - 490, 1991.

[27] (Love, 1944) AEH Love, *A treatise on the mathematical theory of elasticity*, Fourth Ed., Dover Publications, New York USA, 1944.

[28] (Martinelli and Perotti, 2001) L Martinelli, F Perotti, Numerical analysis of the nonlinear dynamic behaviour of sospende cables under turbulent wind excitation, International Journal of Structural Stability and Dynamics 1, 207-233, 2001.

[29] (McConnell and Chang, 1986) KG McConnell, CN Chang, A study on the axial-torsional coupling effect on a sagged transmission line, Experimental Mechanics 26, 324-329., 1986.

[30] (Migliore and Webster, 1979) HJ Migliore, RL Webster, Current methods for analyzing the dynamic cable response, Shock and Vibration Digest, 11, 3-16, 1979.

[31] (Migliore and Webster, 1982) HJ Migliore, RL Webster, Current methods for analyzing the dynamic cable response - 1979 to the present, Shock and Vibration Digest, 14, 19-24, 1982.

[32] (Oliveto and Sivaselvan, 2014) ND Oliveto, MV Sivaselvan, Nonlinear finite element analysis of three-dimensional free and harmonically forced vibrations of stranded conductor cables, Earthquake Engineering and Structural Dynamics 43, 2199-2216, 2014.

[33] (Orawski, 2003) G Orawski, *Overhead Lines*, In: *Electrical Engineer's Reference Book*, Edited by MA Loughton and DF Warne, Elsevier Science, ISBN 0750646373, 2003.

[34] (Paradis and Légeron, 2011) JPH Paradis, F Légeron, Modelling of the free bending behavior of a multilayer cable taking into account the tangential compliance of contact interfaces, Proceedings of the "IX International Symposium on Cable Dynamics", Shanghai (China), 2011.

[35] (Papailiou, 1997) KO Papailiou, On the bending stiffness of transmission line conductors, IEEE Transaction on Power Delivery 12, 1576-1588, 1997.

[36] (Rawlins, 2005) CB Rawlins, *Analytical Elements of Overhead Conductor Fabrication*, Fultus Books, Palo Alto CA(USA), 2005.

[37] (Rawlins, 2009) CB Rawlins, Flexural self-damping in overhead electrical transmission conductors, Journal of Sound and Vibration 323, 232-252, 2009.

[38] (Rega, 2004) G Rega, Nonlinear vibrations of suspended cables - Part I: Modeling and analysis. Part II: Deterministic phenomena, Applied Mechanics Review ASME 57, 443-514 2004.

[39] (Sauter and Hagedorn, 2002) D Sauter, P Hagedorn, On the hysteresis of wire cables in Stockbridge dampers, International Journal of Non-Linear Mechanics 37, 1453-1459, 2002.

[40] (Spak et al., 2013) K Spak, G Agnes, D Inman, Cable Modeling and Internal Damping Developments, Applied Mechanics Review ASME 65, 1-18, 2013.

[41] (Spak et al., 2014) K Spak, G Agnes, D Inman, Parameters for modeling Stranded Cables as Structural Beams, Experimental Mechanics 54, 1613-1626, 2014.

[42] (Urchegui et al., 2008) MA Urchegui, W Tato, X Gómez, Wear Evolution in a Stranded Rope Subjected to Cyclic Bending, Journal of Materials Engineering and Performance 17, 550-560, 2008.

[43] (Utting and Jones, 1987a) WS Utting and N Jones, The response wire rope strands to axial tensile loads - Part I. Experimental results and theoretical predictions, International Journal of Mechanical Sciences 29, 605-619, 1987.

[44] (Utting and Jones, 1987b) WS Utting, N Jones, Response of wire rope strands to axial tensile loads. Part II: comparisons of experimental results and theoretical predictions, International Journal of Mechanical Sciences 29, 621-636, 1987.

[45] (Wang et al., 2015) XY Wang, XB Meng, JX Wang, YH Sun, K Gao, Mathematical modeling and geometric analysis for wire rope strands, Applied Mathematical Modelling 39, 1019-1032, 2015.

[46] (Webster and Mills, 1998) PJ Webster, G Mills, Residual stresses in a steel strand, Physica B 241-243, 1270-1273, 1998.

[47] (Winkler et al., 2015) J Winkler, CT Georgakis, G Fischer, Fretting fatigue behavior of high-strenght steel monostrands under bending load, International Journal of Fatigue 70, 13-23, 2015.

[48] (Zhu and Meguid, 2006) ZH Zhu, SA Meguid, Elastodynamic analysis of low tension cables using a new curved beam element, International Journal of Solids and Structures 43, 1490-1504, 2006.

[49] (Zhu and Meguid, 2007) ZH Zhu, SA Meguid, Nonlinear FE-based investigation of flexural damping of slacking wire cables, International Journal of Solids and Structures 44, 5122-5132, 2007.

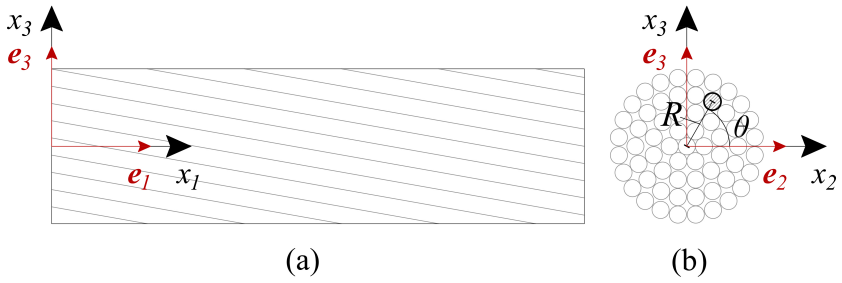

Figure 1: Strand geometry: (a) side view; (b) cross section and definition of the polar coordinates (R, θ).

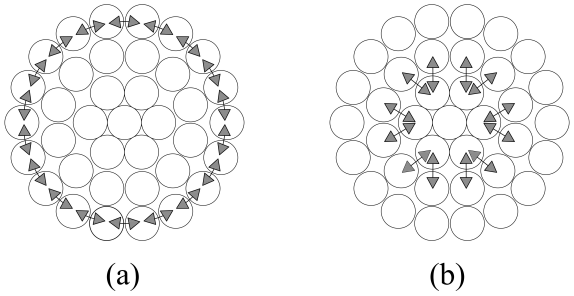

Figure 2: Contact conditions: (a) circumferential contact; (b) radial contact.

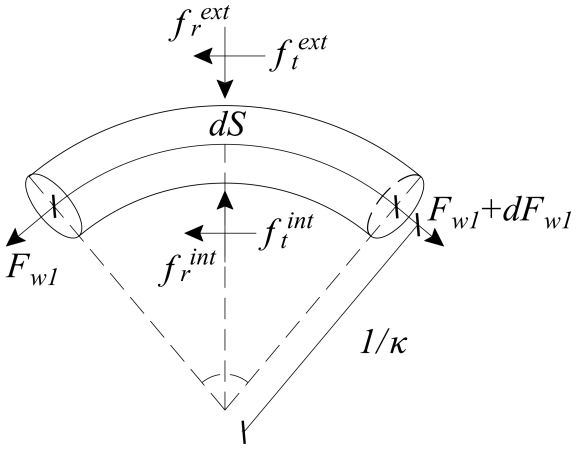

Figure 3: Equilibrium of an infinitesimal wire segment.

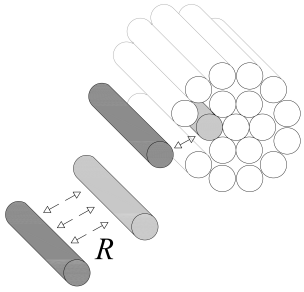

Figure 4: Residual radial forces, R, acting on a wire of the outermost layer.

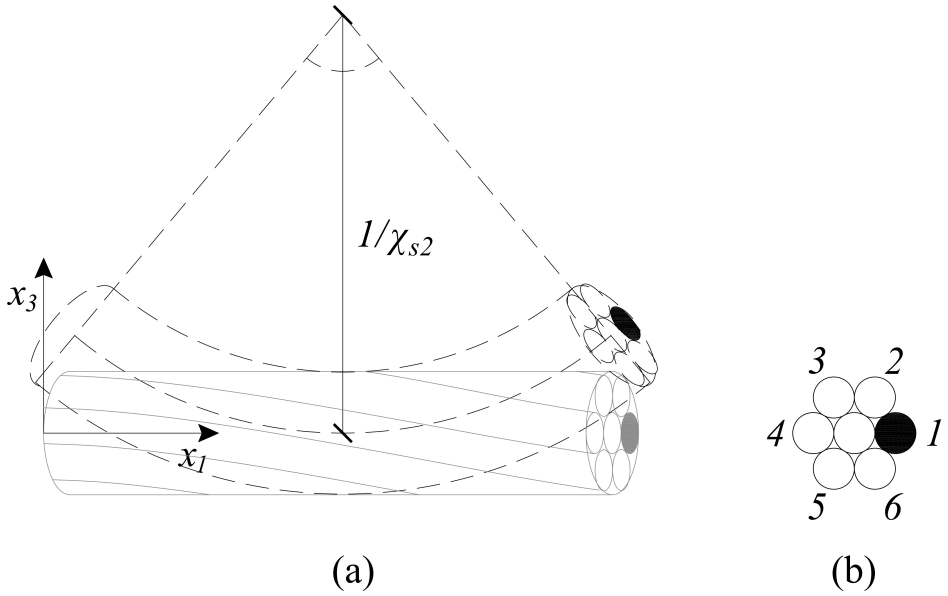

Figure 5: Uniform bending of a 1/6 steel strand: (a) deformative process; (b) cross section of the strand.

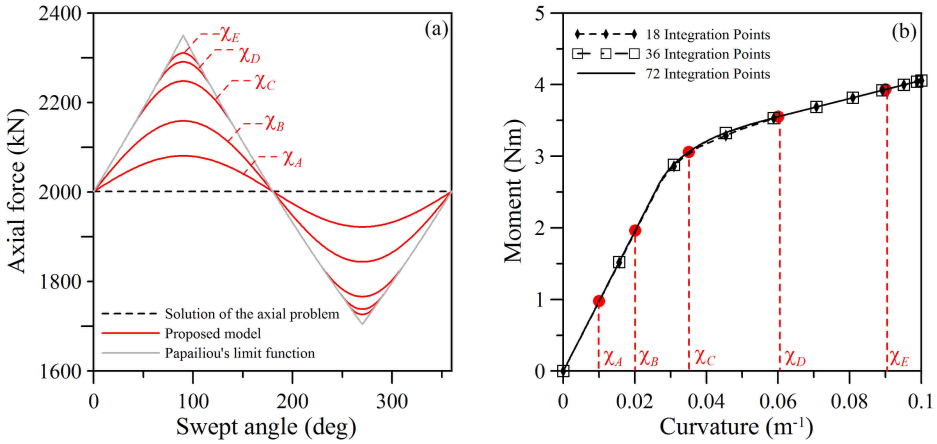

Figure 6: Monotonic bending of the 1/6 steel strand. (a) axial force along the wire 1; (b) cross sectional moment-curvature diagram.

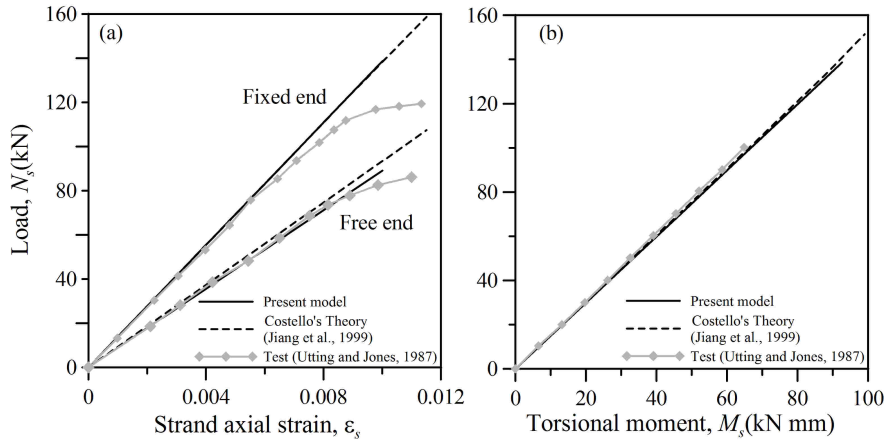

Figure 7: Single layer (1/6) steel strand. (a) Axial load vs. axial strain; (b) axial load vs. torsional moment (fixed end case).

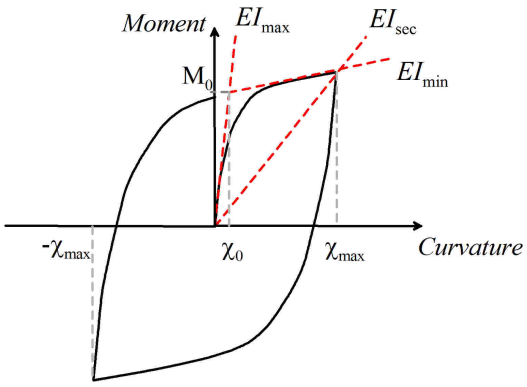

Figure 8: Typical cross sectional bending response computed with the proposed model.

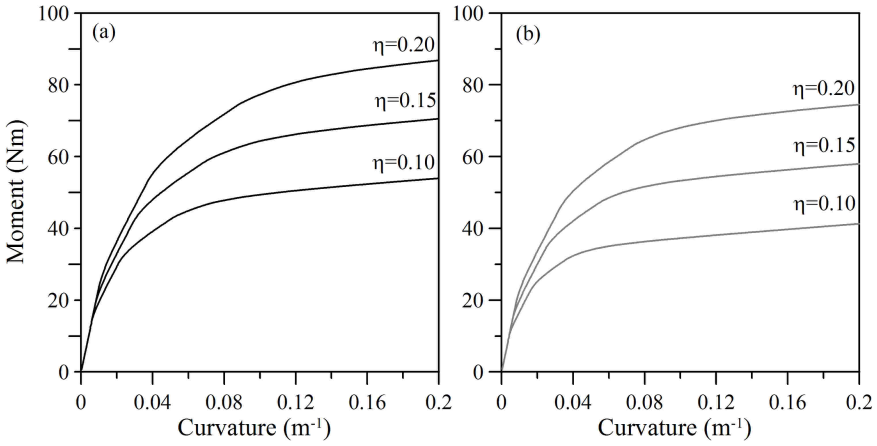

Figure 9: Cross sectional moment-curvature diagrams obtained with the proposed model: (a) with residual contact forces (black line); (b) without residual contact forces (grey line). Friction coefficient: $\mu = 0.7$.

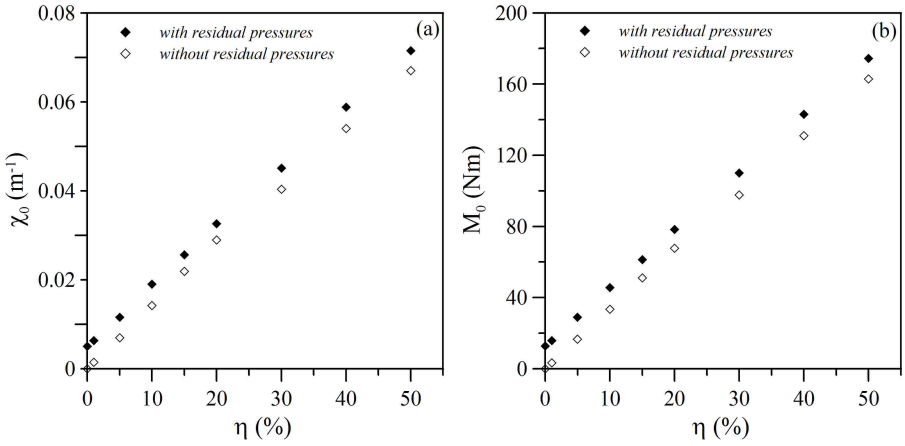

Figure 10: Parameters χ_0 and M_0 obtained with the proposed model as a function of the non-dimensional axial load η. (a) χ_0 vs. η; (b) M_0 vs. η. Friction coefficient: $\mu = 0.7$.

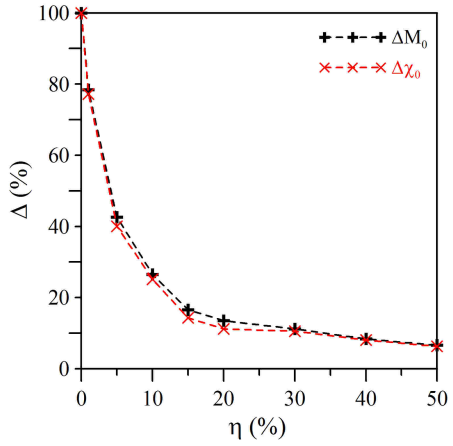

Figure 11: Percentage difference of parameters M_0 and χ_0 evaluated through the proposed model with and without considering the residual contact forces.

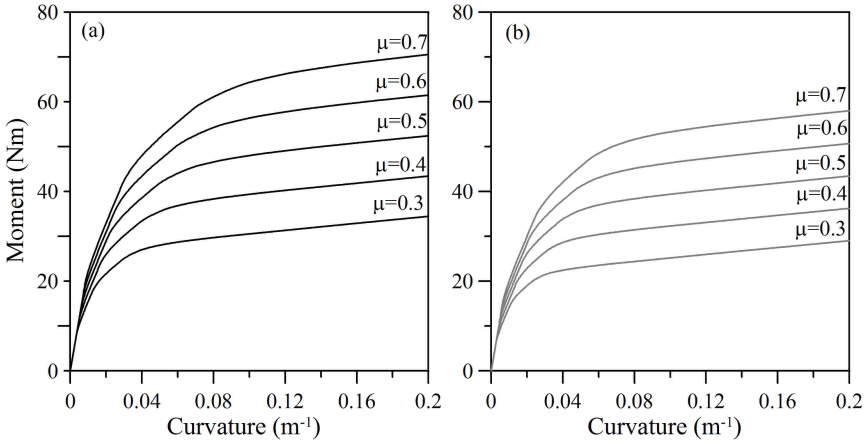

Figure 12: Cross sectional moment-curvature diagrams obtained with the proposed model: (a) with residual contact forces (black line); (b) without residual contact forces (grey line). Non-dimensional axial load: $\eta = 0.15$.

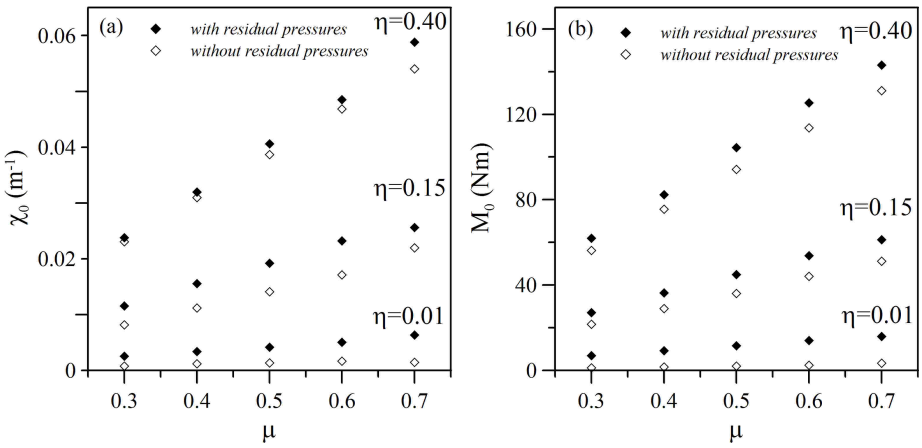

Figure 13: Parameters χ_0 and M_0 obtained with the proposed model as a function of the non-dimensional axial load η. (a) χ_0 vs. η; (b) M_0 vs. η. Non-dimensional axial load: $\eta = 0.15$.

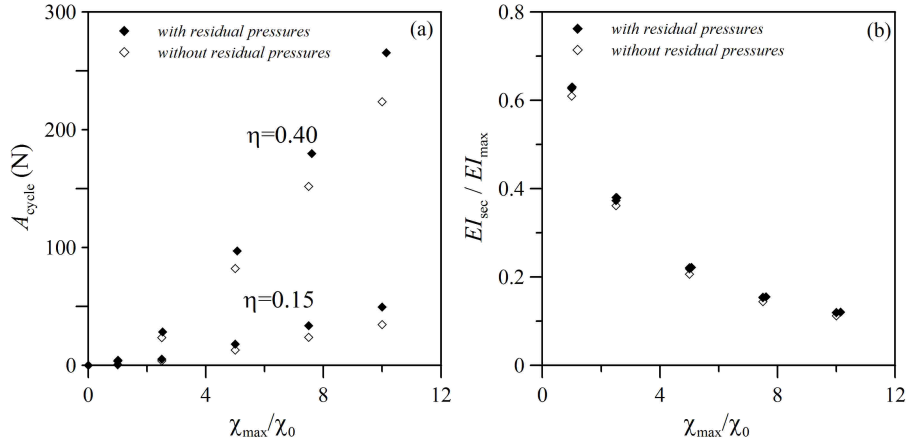

Figure 14: Cross sectional moment-curvature hysteresis loops obtained with the proposed model. (a) Enclosed area; (b) non-dimensional secant stiffness. Friction coefficient: $\mu = 0.7$.

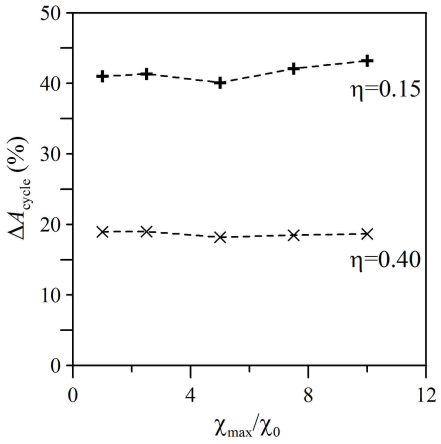

Figure 15: Percentage difference of the area of hysteresis, A_{cycle}, evaluated through the proposed model with and without considering the residual contact forces. Friction coefficient: $\mu = 0.7$.

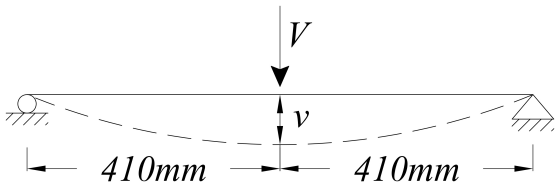

Figure 16: Schematic representation of the experimental test setup.

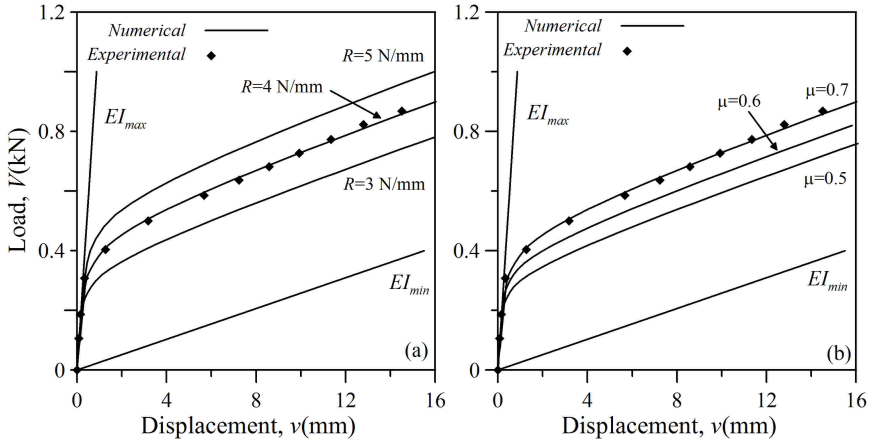

Figure 17: Load vs. displacement at the midspan. Comparison among experimental (dots) and proposed numerical model (continuous lines) results. (a) Friction coefficient: $\mu = 0.7$; (b) residual radial contact force: $R = 4$ N/mm.

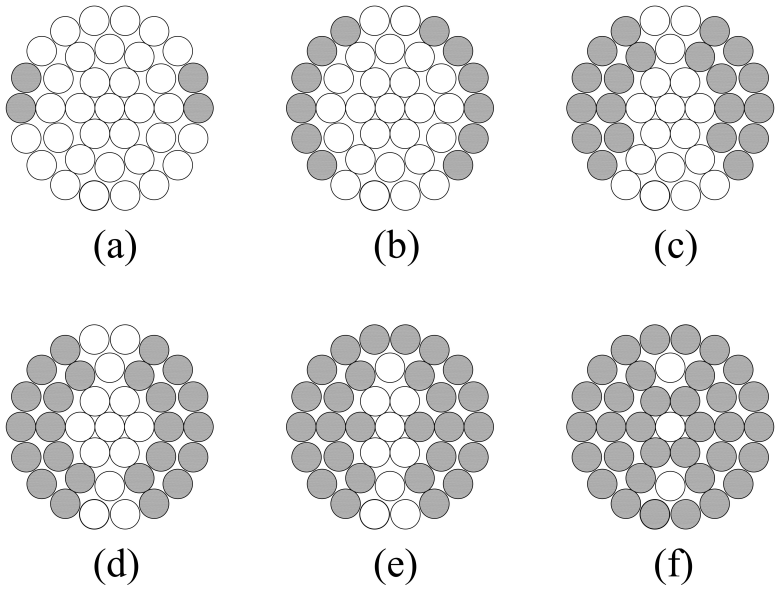

Figure 18: Distribution of wires in slip-state (hatched) for the section at the mid span, in the loading range $V = 200 - 460$ N. Friction coefficient $\mu = 0.7$; residual radial contact force: $R = 4$ N/mm. (a) $V = 200$; (b) $V = 260$; (c) $V = 300$; (d) $V = 360$; (e) $V = 400$; (f) $V = 460$;

Table 1: Single-layer (1/6) steel strand. Geometric and material properties. From (Jiang et al., 1999).

	No. of wires	d **(mm)**	α **(deg)**	**Material**	E **(MPa)**	ν
Core wire	-	3.94	-	*Steel*	188	0.3
Layer 1	6	3.73	11.8	*Steel*	188	0.3

Table 2: Single-layer (1/6) steel strand. Comparison among theoretical and experimental results.

	Proposed Model	**Costello's Theory**	**Experimental**
Fixed end			
$k_1 = \frac{N_s}{\varepsilon_s}$ (kN)	13853	13835	13539
Error $(\%)$	2.32	2.19	-
$k_2 = \frac{N_s}{M_s}$ (1/mm)	1.50	1.52	1.53
Error $(\%)$	2.47	0.822	-
Free end			
$k_1 = \frac{N_s}{\varepsilon_s}$ (kN)	8895	9329	9140
Error $(\%)$	2.68	2.06	-

Table 3: ACSR Curlew 7/54. Geometric and material properties.

	No. of wires	d **(mm)**	α **(deg)**	**Material**	E **(MPa)**	ν	R **(N/mm)**
Core wire	-	3.52	-	*Steel*	200	0.3	-
Layer 1	6	3.52	6	*Steel*	200	0.3	1.671
Layer 2	12	3.52	-10.2	*Aluminum*	69	0.3	0.695
Layer 3	18	3.52	11.7	*Aluminum*	69	0.3	0.399
Layer 4	24	3.52	-14.2	*Aluminum*	69	0.3	0.333